NASA

Technical Memorandum 83840

Accretion Disk Coronae

N. E. White and S. S. Holt

OCTOBER 1981

National Aeronautics and
Space Administration

Goddard Space Flight Center
Greenbelt, Maryland 20771

ACCRETION DISK CORONAE

N.E. White[1] and S.S. Holt

Laboratory for High Energy Astrophysics

NASA/Goddard Space Flight Center

Greenbelt, Maryland 20771

Received 1981 September 28;

ABSTRACT

Recent observations of partial X-ray eclipses from 4U1822-37 have shown that the central X-ray source in this system is diffused by a large Compton-thick accretion disk corona (ADC). We show that another binary, 4U2129+47, also displays a partial eclipse and contains an ADC. The possible origin of an ADC is discussed and a simple hydrostatic evaporated ADC model is developed which, when applied to 4U1822-37, 4U2129+47 and Cyg X-3, can explain their temporal and spectral properties. The quasi-sinusoidal modulation of all three sources can be reconciled with the partial occultation of the ADC by a bulge at the edge of the accretion disk which is caused by the inflowing material. The height of this bulge is an order of magnitude larger than the hydrostatic disk height and is the result of turbulence in the outer region of the disk. The spectral properties of 4U1822-37 and Cyg X-3 are very similar, while 4U2129+47 exhibits a dissimilar spectrum which appears characteristic of Sco X-1/galactic bulge sources; the spectra of all three sources can be reconciled with Compton scattering of the original source spectrum by the

ADC. Spectral variations with the overall intensity state of Cyg X-3 are probably caused by changes in the optical depth of the corona. A consequence of our model is that any accreting neutron star X-ray source in a semi-detached binary system which is close to its Eddington limit is likely to contain an optically thick ADC.

Subject headings: stars: accretion - X-rays: binaries

[1]Also Dept. Physics and Astronomy, Univ. of Maryland

I. INTRODUCTION

The 5.57-hr X-ray binary system 4U1822-37 (Mason et al. 1980) displays a very unusual partial X-ray eclipse, with 50% of the X-ray flux remaining at minimum light (White et al. 1981; hereafter Paper 1). The energy independence of this eclipse led us to conclude in Paper 1 that the compact X-ray source is diffused by a large ($\sim 0.3\ R_0$) Compton-thick highly ionized corona, above and below the center of its accretion disk. This was not the first suggestion for accretion disk coronae (ADC) in compact X-ray binary systems. Jones and Foreman (1976) proposed that the residual emission from Her X-1 during the off part of its 35-d cycle is caused by an ADC scattering X-ray emission from the pulsar around the occulting twisted disk. Subsequent observations have supported this hypothesis (Becker et al. 1977; Pravdo et al. 1979; Parmar, Sanford and Fabian 1980; Bai 1980). In Cyg X-1, Liang and Price (1977) and Bisnovatyi-Kogan and Blinnikov (1977) reconcile the hard X-ray spectrum of this source with disk accretion onto a black hole, by invoking the upscattering of a central source of soft photons in a 10^9 K ADC. These earlier results provided only implicit evidence for the presence of ADCs, whereas 4U1822-37 furnishes a much less subjective experimental signature and indicates that ADCs may have a significant effect on our current understanding of binary X-ray sources in general.

We will show that another X-ray source, 4U2129+47, is diffused by an ADC and hence appears extended to an outside observer (II). A simple model for an evaporated ADC is developed and shown to be consistent with the observed coronae (III and IX). The observed eclipse duration and depth are used to determine the coronal radius and the nature of the secondary in 4U2129+47 and 4U1822-37 (IV).

In addition to the eclipse, 4U1822-37 also exhibits a 50% peak-to-peak

secondary modulation, with its minimum occuring at phase ~ 0.2 prior to the eclipse center. In paper 1 we pointed out that this modulation is very similar to the 4.8-hr modulation of Cyg X-3. A similar effect is also apparent in new X-ray observations of 4U2129+47. We will further explore the possibility, discussed in Paper 1, that the secondary modulation results from the occultation of the ADC by structure at the periphery of the accretion disk caused by the inflowing gas stream (V and VI). The spectral properties of Cyg X-3, 4U1822-37, and 4U2129+47 are presented and discussed in the context of previous models for Cyg X-3 and the ADC model proposed here (VII). Finally, the implications of our results as regards the nature of the galactic bulge sources is discussed (X).

II. NEW 4U2129+47 DATA

The optical light curve of 4U2129+47 is modulated with a period of 5.2 hrs and an optical spectrum which is cooler at minimum light suggests that it results from the rotation of an X-ray heated secondary, similar to HZ Her (Thorstensen et al. 1979). This is in contrast to the optical counterpart of 4U1822-37, which shows the color-independent eclipse of an accretion disk (Mason et al. 1980). Ulmer et al. (1980) have reported evidence for an X-ray eclipse of 4U2129+47 coincident with the optical minimum. Using the HEAO-1 A2[+] experiment we have obtained three 10-day scanning observations in Dec

---

[+]The A2 experiment on HEAO-1 is a collaborative effort led by E. Boldt of GSFC and G. Garmire of CIT, with collaborators at GSFC, CIT, JPL and UCB.

1977, June 1978 and Dec 1978 and one 3-hr pointed observation on 1978 Nov 28 (see paper 1 for instrument details). In May 1979 we made a 4-hr observation using the SSS and MPC detectors on the Einstein Observatory HEAO-2.

The folded HEAO-1 A2 count-rate data are shown in Figure 1, and the Einstein data in Figure 2, both with the non-source background removed, and plotted against the orbital period ephemeris given by Thorstensen et al. The X-ray eclipses at phase zero are evident in all the data, with a 25% residual flux at minimum. The eclipse data with the best statistical quality that we have, from the MPC/SSS, show an extended ingress lasting at least 0.1 in phase (Figure 2). The MPC hardness ratio (the flux in the 3.3-10.0 keV band to that over 1.1-3.3 keV) indicates a slight hardening of the spectrum through the eclipse. Spectral fits to the MPC data show a small increase in absorption from $<1.3 \times 10^{21}$ to $3.2 \pm 1.0 \times 10^{21}$ H atoms cm^{-2}, while similar fits to the SSS data give only an upper limit to ΔN_H of $< 2 \times 10^{21}$ H cm^{-2}.

Three possible explanations for a partial eclipse were discussed in paper 1: a) The grazing occultation of a stellar X-ray source by its companion, b) immersion of the system in a stellar wind, or c) an ADC surrounding and diffusing the X-ray emission from the source. The energy independence of the partial eclipse of 4U1822-37 eliminated the first two models for that system. Even if the small increase in absorption seen by the MPC from 4U2129+47 during eclipse is significant, it is still at least one order of magnitude below that expected from the first two models (see paper 1), so we conclude that the emission from 4U2129+47 is also diffused by an ADC.

III. ACCRETION DISK CORONAE (ADC)

Several workers have proposed that the accretion disk surrounding a compact X-ray source will be sandwiched between a hot corona. Models for generating an ADC can be divided into two groups: the dissipation of acoustic or magnetic energy flux generated by convective or viscous turbulence within the disk, or the evaporation of disk material by the central source.

Icke (1976) first suggested that the viscous turbulence within an

accretion disk, responsible for the transport of angular momentum outwards, could also give rise to acoustic noise in the disk and generate a hot corona (analogous to similar models for the solar case). In the same vein, Bisnovatyi-Kogan and Blinnikov (1977) and Liang and Price (1977) discuss convective turbulence in the inner photon-pressure-dominated region of an accretion disk (see also Galeev, Rosner and Vaiana 1979), although the photon pressure region is in the innermost region of a disk and is much smaller than the coronal radii under consideration here. Most of the accretion disk surrounding any compact object (including a neutron star or white dwarf) will be gas-pressure-dominated, and it is unclear whether convective instabilities can generate a corona in such a situation (Tayler 1980; Shakura, Sunyaev and Zilitinkevich 1978; Livio and Shaviv 1977), or what the contribution from viscous turbulence will be (Icke 1976). In addition, there may be magnetic loops threading the disk, again analogous to the solar case. Because of these uncertainties we will concentrate on the other possibility, an evaporated ADC.

Shakura and Sunyaev (1973) pointed out that the central source in an X-ray binary system will evaporate material from the surface of its accretion disk. If it does not escape from the system, this hot material then settles above and below the disk as a corona. The physics of this process has been thoroughly discussed with regard to the self-excited stellar wind mechanism for causing mass transfer in X-ray binaries (e.g. London, McCray and Auer 1981 and refs therein). These calculations can be used to predict the properties of an evaporated ADC.

When the atmosphere of a star or an accretion disk is illuminated by a source of X-rays it will photo-absorb the incoming radiation and re-emit the energy as continuum and line emission. The bremsstrahlung cooling per unit mass is proportional to $n\sqrt{T}$, while the heating per unit mass depends only on

the ionization state of the gas, not its density; therefore $n \propto T^{-1/2}$. The equation of state, however, gives $n \propto PT^{-1}$, i.e. $n \propto P^{-1}$ and, for hydrostatic equilibrium, the gas is thermally unstable. At sufficiently low densities an equilibrium can only be achieved by abruptly raising the gas temperature to change its ionic state, thereby reducing the X-ray heating (e.g. McCray and Hatchett 1975). The presence of line cooling will complicate this simple picture somewhat, but does not change the overall result. If the thermal energy of the gas exceeds the gravitational energy then a stellar wind is formed. If not, surrounding an accretion disk there may be a large volume where material within the radius $R_E \sim (M_X/M_O)$. T_7^{-1} R_O will remain in hydrostatic equilibrium. The coronal temperature T_7 in units of 10^7 K is given by the balance between bremsstrahlung losses, Compton cooling and Compton heating. For the case in which we are interested, the bremsstrahlung is negligible and, from Shakura and Sunyaev (1973), we obtain $T_7 = 0.25\ T_s$, where T_s is the central source temperature. T_s is unknown but we will assume it to be similar to that measured from X-ray pulsars and set $T_s = 24$ (appropriate for Her X-1), consistent with the value used by McCray and Hatchett, but note that the value of T_s may noticeably change the size of the coronal region from source to source. The density structure of the corona as a function of the angle from the plane of the disk θ at a radius R can be obtained by equating the gas pressure to the net gravitational and radiation pressure (after Lynden-Bell 1969). The resultant gas density n is Gaussian-distributed about the accretion disk plane as,

$$n = n_{max} \exp\left(- \frac{(R\theta)^2}{2b^2} \right) \qquad (1)$$

where

$$b^2 = 10^7 . \frac{kT_7 R^3}{GM_x \mu} \left[1 - \frac{L_x}{L_{edd}} \right]^{-1}$$

and L_{edd} is the Eddington-limited luminosity for a source of mass M_x. The critical density at which line cooling becomes important is the maximum density n_{max} possible at the base of the corona where the high temperature is maintained. n_{max} is determined solely by L_x and R, the luminosity of and the distance from, the X-ray source. This corresponds to an ionization parameter ξ of $\sim 10^4$ (McCray and Hatchett 1975) such that

$$n_{max} = 4 \times 10^{12} . \frac{L_x}{L_{edd}} . \left(\frac{R_\odot}{R} \right)^2 \text{ cm}^{-3} \qquad (2)$$

for a 1.4 $M_\odot$ neutron star.

An estimate of the optical depth τ through the corona at high inclinations ($i=90^\circ - \theta$) may be obtained by integrating (2). The luminosity L_c, above which the corona becomes optically thick is

$$L_c = 5 . L_{edd} . (R_{in}/R_\odot) \text{ erg s}^{-1} \qquad (3)$$

where R_{in} is the inner radius of the corona. The low density of the corona will probably prevent it extending all the way in to the Alfven surface and it will be disrupted by the magnetic field at some point within the "transition zone" (discussed in Ghosh and Lamb 1980) and R_{in} will be $\sim 10^{-2}$ $R_\odot$. Therefore an ADC will be Compton-thick only for $L_x/L_{edd} \gtrsim 0.1$. The optical depth as a function of inclination is shown in Figure 3 for an arbitrary value of R_{in} = 0.05 $R_\odot$ and T_7 of 6. For $L_x/L_{edd} \gtrsim 0.1$ the source will always be

obscured ($\tau > 1$) above inclinations of 60^0, and might possibly be at lower inclinations as well, depending on the density (which is specified by L_x). For $\tau > 1$ the photon density at a given distance R will be enhanced because photons will be trapped in the corona for the time that it takes them to escape. Ross (1979) has shown that in this case the true luminosity of the X-ray source cannot be ascertained without concurrent knowledge of the density structure. For our discussion the interior modelling of the ADC is not important; we require only the conditions to produce an ADC. In Figure 4 the probable appearance of the evaporated ADC corona of 4U1822-37 is illustrated.

IV. THE ECLIPSE BY THE SECONDARY

All the eclipse calculations have been performed via numerical rather than analytic means. In order to model the eclipses observed in these systems it is useful to define the dimensions of the optically thick region of the corona as they would appear to an outside observer. This can be done by considering the "surface of last scattering" defined as the radius R_c (perpendicular to the line of sight) and height H_c (parallel to the disk) at which $\tau = 1$ (cf Fabian and Pringle 1978). Numerical integration of (1) and (2) gives

$$H_c \approx 0.5\left(\frac{R_c}{R_o}\right)^{1.5} \cdot T_7^{1/2} \; R_o \qquad (4)$$

Most of the subsequent analysis is relatively insensitive to uncertainties in (4) but we shall indicate where our results depend on it. Two further assumptions were made: (1) a spherical secondary that fills its Roche lobe, so that its mass M_s and radius R_s are related by the Roche mass-radius relations given by Paczynski (1971), and (2) the X-ray source is an accreting

neutron star with $0.8 < M_x < 2.0\ M_\odot$. These two assumptions, Keplers third law and (4) make the duration and depth of the eclipse functions of only i, R_s and R_c.

The results of fitting the secondary eclipses of 4U1822-37 (taken from the HEAO-1 A2 pointed observation, paper 1) and 4U2129+47 (MPC data, Figure 2) are given in Figure 5 as R_s vs i and R_c vs i. From Figure 5 it is apparent that the radius of the ADC corona is insensitive to both the companion radius and the system inclination, and that the coronal radius in 4U1822-37 at least half that of 4U2129+47. The constraints imposed by the eclipse on the nature of the secondary i: these two systems are as follows:

(1) 4U1822-37: The statistical errors are dominated by the uncertainty in the mass of the compact object (assumed in Figure 5 to be $0.8 < M_x < 2.0\ M_\odot$). The error associated with any possible uncertainty in the coronal height is much smaller than this. A hydrogen zero age main sequence (ZAMS) secondary gives $i \approx 75^\circ$. If the inclination is $\gtrsim 85^\circ$ then the mass of the secondary will be less than $0.085\ M_\odot$, the minimum value for hydrogen nuclear burning. However, a degenerate secondary that fills its Roche radius exceeds the maximum theoretical radius for a cold hydrogen white dwarf ($\sim 0.1\ R_\odot$, Zapolsky and Salpeter 1969) and limits $i < 85^\circ$. For $i \lesssim 67^\circ$ the secondary would be a helium star, however the detection of hydrogen emission in the optical spectrum makes this unlikely (Mason, private communication).

(2) 4U2129+47: We have high quality (pointed) coverage for only one third of the eclipse and the statistical errors for R_c and R_s are comparable to those from the uncertainty in the mass of the X-ray source. The error region in Figure 5 for this source is defined from only the statistical uncertainties, and the error region moves to the left or right as the X-ray source mass changes. Because the coronal radius is so large this solution is

sensitive to the assumed coronal height. We used a height of 0.4 R_0; for lower values the solution does not change significantly, but for greater values it gives larger secondary radii for a given inclination. Degenerate secondaries are ruled out for all possible solutions. A helium star is also unlikely because of the observed color variations and H line emission (Thorstensen et al. 1979). A hydrogen ZAMS sequence secondary gives $i \sim 82^{o}$. A larger coronal height than that assumed will, for a given mass radius relation for the secondary, move i closer to 90^{o}. We note that the shape of the eclipse center is quite dependent on the coronal height used, so that a complete observation of the whole eclipse with high statistical precision should remove any uncertainty concerning the coronal height.

V. THE ECLIPSE BY AN ACCRETION DISK BULGE

The periodic hump seen in the light curves of many cataclysmic variables is believed to come from a hot spot at the point of impact of the inflowing gas stream with the edge of the accretion disk (e.g. Robinson 1976). Intense flickering of the light from the hot spot suggests turbulence and this may cause a thickening of the disk in the vicinity of the hot spot (e.g. Lubow and Shu 1976). Chester (1979) and Alpar (1979) have modelled the time delay of the optical pulse from DQ Her (outside eclipse) in terms of a reprocessed pulse on the outer disk surface and both found a thickening of the trailing edge of the disk, although the vertical extent of this structure was not determinable. Hassall et al. (1981) have suggested a similar scheme to account for the reprocessed optical pulses from H2252-035. Periodic absorption dips from 4U1915-05 have been explained in terms of the occultation of the X-ray source by a structure on the outer edge of the disk (White and Swank 1982; Walter et al. 1982). A gradual decline in the light from the optical counterpart to 4U1822-37, prior to the eclipse of the accretion disk

by the secondary, may be caused by a bulge, near the hot spot, occulting part of the disk (Mason et al. 1980), where the hot spot in this case is relatively dark compared to the X-ray-illuminated disk. This bulge may also occult the ADC and cause the sinusoidal-like modulation of the X-ray flux (Paper 1).

A number of similarities between the X-ray properties of 4U1822-37 and Cyg X-3 were given in Paper 1, where it was suggested that they might be intrinsically similar systems (see also VIII). Our simple description "a quasi-sinusoidal modulation" glosses over several interesting details that deserve more attention, and a self-consistent picture should be capable of explaining their differences, as well as their similarities. The minimum in the light curve of Cyg X-3 is asymmetric, with a steeper fall than recovery (e.g. Mason et al. 1976a, and Figure 9). 4U1822-37 displays a different behavior with a more gradual decline to minimum, a steeper rise to a plateau where the eclipse by the secondary occurs and then a second increase to maximum light (Figure 6 this paper; Figure 1 paper 1). These features have remained constant over many years (Elsner et al. 1980 and paper 1).

In this section we investigate the possibility that both these modulations are caused by occultation of the ADC by azimuthal variations in the height of the outer edge of the accretion disk. The numerical code used to model the eclipse by the secondary was modified to include an occultation by material at the periphery of the disk. In all these calculations we assumed the standard thin disk radius-height relation of $H_d = 0.05\ R_d^{1.125}$ (corresponding to an outer disk temperature $T_D = 2 \times 10^4$ K) and that the bulge is confined to the edge of the disk. We used the thin disk relation for convenience and note that the disk may be thicker. The following results are independent of reasonable variations in the height-radius relation of the disk, or of the coronal radius-height relation.

A simple bulge profile (shown at the bottom of Figure 6) that had a sharp rise at the confluence of the gas stream with the disk and decayed linearly downstream of that point was tried first. Two parameters modified the shape of the resulting light curve for this geometry: a) the rate of decay of the bulge with azimuthal angle and b) the ratio of the radius of the optically thick region of the corona to that of the disk. Figure 6 shows the effect of increasing R_c, keeping the other parameters, in particular the disk radius, constant. The secondary eclipse has been removed for clarity and the HEAO-1 A2 pointed observation of 4U1822-37 is given (but not fit) for comparison. R_c well inside R_d gives a sharp minimum, but as the coronal radius approaches the disk radius the minimum becomes shallow, with a slight asymmetry similar to that of the Cyg X-3 light curve. This simple geometry cannot, however, reproduce either the plateau around the secondary eclipse in 4U1822-37 or the duty cycle of the modulation of Cyg X-3.

The plateau in the light curve of 4U1822-37 suggests a thickening of the disk near $\Phi = 0$, i.e. upstream from the confluence. Including such a thickening in the prebulge region gives light curves such as those shown in Figure 7. As R_c approaches R_d this plateau becomes smeared out and again we obtain a smooth light curve, but now with a longer duty cycle similar to that of Cyg X-3. Figure 7 indicates that all the gross features of the light curves of both Cyg X-3 and 4U1822-37 can be reproduced with the same model, with their differences arising primarily from the distance between the bulge and the optically thick edge of the corona.

a) The X-ray light curve of 4U 1822-37

Formal fits to the data were made with the the angle of confluence δ, the bulge height above the plane of the orbit H_B, the phase angle through which it linearly decays θ_D, the phase angle of the start of the prebulge θ_p and the

prebulge height H_p as free parameters. The top panel of Figure 8 shows an optimized light curve for this geometry. We note that the minimum thickness at phase ~ 0.25 is similar to that found by Chester and Alpar for DQ Her (at $\phi \sim 0.7$ using their phase convention). However, there are still systematic deviations from the predicted light curve that suggest the prebulge region is not constant in height, but decays in the same sense as does the primary bulge (with a phase angle through which it decays of θ_{D2}). This modification improves the predicted light curve considerably, as shown in the second panel. χ^2 is formally unacceptable at 410 for 163 dof for this fit, but because of turbulence the bulge shape is probably fluctuating on timescales much shorter than an orbital period. A sharp rise was used for the start of the bulge at the confluence. In reality this feature must be less abrupt and the inclusion of a more gradual rise did not significantly change the resulting light curves.

It might be argued that the light curve is being over-modelled, i.e. given enough parameters any random light curve can be reproduced, but not all physically reasonable alternatives lead to better fits. A large number of bulge profiles were tried, including gaussian and exponential decays, prebulges that increase in height downstream, and a highly elliptical disk (widest perpendicular to the line joining the two stars) but none synthesized the features of the observed light curve.

The only other high quality data of 4U1822-37 available comes from an Einstein MPC observation made one year later. The data are shown in the third trace of Figure 8, with the best fit HEAO-1 A2 light curve. The data are sparse, but the general features of the light curve are confirmed, although there is evidence that the angle δ may have changed slightly. The best fit parameters for 4U1822-37 are given in Table 1. The inclination was varied

from 70^{o} to 80^{o}, which gave a range of bulge height of 0.15-0.3 R_{o}, but no other parameters were affected by changing the inclination. Because the coronal radius is fixed by the secondary eclipse, we can determine a radius for the disk of 0.6-0.7 R_{o}. The proposed geometry for 4U1822-37 is illustrated in Figure 4.

b) The Optical and UV Light Curves of 4U1822-37

The optical light curve consists of a gradual decline from $\phi \sim 0.6$ - 0.9, followed by a relatively sharp eclipse of the accretion disk by the secondary. Mason et al. (1980) suggested that the pre-eclipse decline is caused by an occultation of the central region of the disk by a bulge at the edge of the disk. The numerical code was modified to model the expected optical eclipse using the azimuthal bulge profile from the X-ray data, assuming that the disk interior (including the bulge) is uniformly bright, and that the outside rim of the disk, not exposed to the X-ray source, is dark relative to the disk interior. The optical data from Mason et al. (1980) are shown in Figure 8. The dashed line is the predicted light curve assuming no additional light in the system. There is a minimum at phase 0.8, but it is much deeper than the observed decline. This is because the light curve is made up of a combination of both the occultation of the disk by the bulge, and the self occultation of the bulge itself which, at such high inclinations, contributes a sizable fraction of the light. The effect of adding additional light from the secondary is shown as the solid line; 40% of the total light is assumed to be from an X-ray heated secondary and is modulated by 100%. The resultant light curve is closer to the predicted light curve, but it still is not satisfactory. Therefore, while the pre-eclipse decline can probably be accounted for by the effects of viewing the bulge at different binary phases, the white light data must be complicated by either a non-uniform distribution

of light across the disk, or additional light from the hot spot/gas stream. We can obtain limits on the radius of the accretion disk from the white light eclipse in a manner similar to those obtained for the ADC radius, and find R_d = 0.7±0.1, consistent with the value found from the X-ray light curve. It is interesting to note that a second minimum at phase 0.5 may correspond to a partial eclipse of the secondary by the accretion disk (cf. Longmore et al. 1981).

Mason and Cordova (1982) have recently obtained a coarsely binned measurement of the far UV light curve (in seven binary phase intervals) and find that it resembles the X-ray light curve with a minimum at $\phi \sim 0.9$, although with a larger amplitude. This is in good agreement with the modelling in Figure 8 and suggests that the far UV comes entirely from the X-ray illuminated accretion disk and is uncontaminated by the other light sources.

In paper 1 evidence was given for a phase shift between the X-ray and optical minima, with the optical leading the X-ray by 0.04 in phase. In order to correctly center the predicted secondary eclipse, the optical data shown in Figure 8 is phase shifted by 0.015 from that of Mason et al (1980), which is within the 0.018 phase uncertainty of the current ephemeris (Paper 1). The remaining phase difference between the X-ray and optical epochs indicates that the distortion of the eclipse caused by the pre-eclipse decline has biased the definition of the center of the optical minimum.

c) Cyg X-3

The azimuthal profile for the disk used to fit 4U1822-37 was applied to an average light curve of Cyg X-3, taken from MPC data obtained during an Einstein observation in Dec 1978 (the same data used by Elsner et al. 1980). The source was in a very low state (~ 50 UFU) and exhibited variations in the

light curve from cycle to cycle (see Figure 1 of Elsner et al.). The data and best fit light curve are shown in Figure 9. The general trends of the modulation are reproduced remarkably well and the formally unacceptable χ^2 is understandable in terms of variations in the light curve on short timescales well in excess of the excellent statistics. Apart from the bulge height, the only changes made to the 4U1822-37 azimuthal profile were a decrease in θ_D to 100^o and an increase in θ_p to 290^o. The ratio of the prebulge height to the primary bulge was the same for both source fits. Because we have no prior knowledge of the coronal radius, we can obtain only a range of bulge heights as a function of the ratio R_c/R_d which, as expected, was larger than the values for 4U1822-37 ($\sim$ 0.75 vs 0.5). Figure 10 displays the predicted bulge height as a function of inclination for different disk radii. The arbitrary phase in Figure 9 has Φ=0 corresponding to approximately where the eclipse by the secondary would occur if $\delta \sim 40^o$.

The lack of any eclipse places an upper limit on the secondary radius as a function of inclination. This is indicated in Figure 10 assuming M_x = 1.4 M_o. The 4.8-hr orbital period of Cyg X-3 means that a Roche-filling cold 100% hydrogen white dwarf is just possible (see Elsner et al. 1980), but the white dwarf would be of an extremely low mass $\sim$ 0.005 M_o and on the verge of becoming a planet (Zapolsky and Salpeter 1969). The improbability of such a large mass transfer rate ($L_x \sim 10^{38}$ ergs s^{-1}) occuring in such a system suggests the secondary is not degenerate, which limits $i < 80^o$. A hydrogen ZAMS secondary gives $i < 68^o$.

The average luminosity of Cyg X-3 in the 2-10 keV band can vary by a factor 5 on timescales of months. Five days of HEAO-1 A2 scanning observations of Cyg X-3 in its high state in 1978, folded at 4.8-hrs, are displayed in Figure 9. The scatter in the data points is greater than that in

the MPC data because the observation is over such a long time interval and the source is only seen for ~ 1 minute out of every 40, so that it is very susceptable to local fluctuations in the source intensity. Nonetheless the general shape demonstrates that there have been no major change in the coronal radius or the bulge height.

Determination of the bulge height above the disk in Cyg X-3 is dependent on knowledge of the disk radius and system inclination. From Figure 10, the peak bulge height in Cyg X-3 must be at least half of the disk radius or $\gtrsim$ 15 times the hydrostatic disk thickness (for T_D = (.6-2) x 10^4 K) and subtends an angle of > 40^0 to the central source. This compares with the 4U1822-37 value of about one third the disk radius or ~ 7-15 times the hydrostatic thickness, subtending an angle of ~ 20^0 to the central source.

d) 4U2129+47

The statistical quality of these data do not constrain the model as severely as do those from Cyg X-3 and 4U1822-37, so that no rigorous attempt has been made to model its light curve. However, the overall light curve of 4U2129+47 seen on 1977 day 342-352 does bear a marked resemblance to the quasi-sinusoidal modulation of 4U1822-37, with a second minimum occuring at phase ~ 0.65 (Figure 1). This minimum is not as obvious six months later (where the statistics are worse), and is not at all evident in either the pointed or scanning HEAO-1 A2 data when the source was at a factor 2 lower intensity. In May 1979, the source returned to its higher intensity and a second minimum again seems to be present, but at a slightly later phase of ~ 0.75 (Figure 2). The possible shift in the phase of the minimum indicates the tantalizing possibility of major changes in the outer disk structure, possibly related to the change in X-ray intensity. This source clearly deserves further attention from X-ray observers.

VI. THE NATURE OF THE BULGE

The accretion disks in systems such as these are a consequence of the necessity for the loss of angular momentum before accretion onto the compact object can occur. Flannery (1976) and Lubow and Shu (1975) suggest that the equilibrium outer radius of the disk R_M is given by the point at which the specific angular momentum of the disk material equals that of the infalling material. If the disk radius differs from this, then a large velocity differential occurs across the confluence and causes strong turbulence that tends to spin the disk up or down, accordingly. Tabulated values for both R_M and the angle of confluence δ are given in Lubow and Shu and Flannery and we can compare them with the observed disk values for 4U1822-37. Mass ratios M_x/M_s in the range 1 to 10 give R_M between 0.15 and 0.49 R_o, which is significantly less than the disk radius estimates for 4U1822-37 of 0.6-0.7 R_o. Further evidence that the disk in 4U1822-37 is larger than the equilibrium value is given by δ which is $\sim 20^o$ below that expected for the given mass ratio range. So, unless the mass ratio in this system is extremely large (i.e. the compact object is $\gg 2\ M_o$), the disk radius must be about twice R_M. Therefore, large slip velocities and turbulence may be expected at the confluence.

Turbulence will increase the effective gas pressure within the disk and cause the disk to thicken at its edge. The turbulent pulsation gas pressure P_t is given by ρV_t^2 where ρ is the density and V_t the mean velocity of the turbulent motion. This increases the scale height of the disk by a factor T_H given by

$$T_H = \left[1 + \left(\frac{\omega}{\gamma}\right)^2\right]^{1/2} \approx \omega \qquad \text{for } \omega > 1 \qquad (6)$$

where ω is the turbulent Mach number and γ the ratio of specific heats (Shakura, Sunyaev and Zilitinkevich 1978). V_t is unknown but should be comparable to the velocity difference ΔV across the confluence and must be less than the keplerian velocity. The sound speed in the disk will be ~ 10 km s^{-1} and is much less than the outer disk keplerian velocity of ~ 600 km s^{-1}. An ω of 7 to 15 for 4U1822-37 gives a V_t ~ 100 km s^{-1}. The factor-of-two larger bulge height for Cyg X-3 can be accounted for by a different mass ratio and/or disk size, either of which can increase ΔV across the confluence. At such large Mach numbers the gas pressure will be increased by vorticity caused by the generation of shock waves in the turbulance, further thickening the disk. It is unclear how far into the disk the turbulence will penetrate. Such large supersonic turbulent velocities must lead to fluctuations in the size and shape of the bulge consistent with the observed cycle-to-cycle variations in the structure of the light curve of Cyg X-3. These variations tend to occur predominantly on the rise and peak of the 4.8-hour cycle (van der Klis, priv. comm.; Parsignault et al. 1976), suggesting that the most dramatic variations in the disk height occur in the region upstream from the confluence, i.e. in the structure of the second bulge. The longer term variations in the light curve seen by van der Klis and Bonnet-Bidaud (1981) may reflect changes in the coronal radius, disk radius or disk structure. Bonnet-Bidaud and van der Klis (1981) have also recently found evidence for a 20-day 1% periodic phase shift in the times of minimum light from Cyg X-3. This suggests that there may be a slight oscillation in the position of the bulge.

The accreting material is spun up to the disk velocity and injected into orbit about the compact star, but the second bulge indicates that it is an orbit that intersects stable orbits of disk material, which causes it to

collide with the disk a second time, giving rise to another shock (similar to shock II in Lubow and Shu). The three-body hydro-dynamics of this situation are complicated, however, we note that this first direct measure of the azimuthal structure at the edge of an accretion disk provides an important constraint to any general description of disk accretion.

Smak (1979) and Sulkanen, Brasure and Patterson (1981) have measured the radii of the accretion disks in several cataclysmic variables (CVs) and found them all to be substantially larger than R_M. We might, therefore, expect large bulges in CVs as well, and it is perhaps a little puzzling why such prominent features may have gone unnoticed in such well-studied systems. The outer thickness of the disk is determined by its temperature and part of the explanation may come from X-ray heating enhancing the thickness of the outer disk structure. Further, for high inclinations the luminosity of the hot spot can be comparable to that of the disk (Bath et al. 1974), and the characteristic hump in the light curve from the spot could be masking the pre-eclipse decline (like that seen in 4U1822-37) caused by the self-occultation of the disk by the bulge.

RW Tri is a CV whose orbital period (5.57-hrs) and dynamic properties are very similar to those of 4U1822-37. Longmore et al. (1981) have recently observed an IR eclipse of the secondary by the accretion disk and from this they estimate a radius for the disk of $\sim 0.75\ R_O$, or five times R_M. They also measure a "surprisingly large" thickness for the disk of 0.11-0.17 R_O. The disk thickness we measure in 4U1822-37 at $\Phi \sim 0.0$ and $\Phi \sim 0.5$ (see the bulge profile in Figure 8) is very similar to that seen by Longmore et al. Therefore, such large bulges may be a common phenomenon in CVs and low mass X-ray binaries.

VII. SPECTRAL RESULTS

Non-dispersive X-ray spectra of Cyg X-3, 4U1822-37 and 4U2129+47 were obtained using HEAO-1 A2 and the Einstein SSS. The HEAO-1 A2 data come from two independent detectors sensitive in overlapping and complementary energy bands 2-20 keV and 2-60 keV, each with 64 channels of PHA. The SSS covers the range 0.5-4.5 keV with 128 channels of PHA, and has a factor 4 better energy resolving power at 3 keV than do the HEAO-1 A2 detectors. Additional spectral information out to ~ 20 keV is provided by eight channels of PHA from the Einstein MPC. All uncertainties are 90% confidence.

a) Cyg X-3

The spectrum of Cyg X-3 changes radically from its low to high state (Serlemitsos et al. 1976; Sanford, Mason and Ives 1976) and this has caused some confusion regarding the spectral properties of this source (cf Becker et al. 1978; Blisset, Mason and Culhane 1981)

The low state HEAO-1 A2 results come from a pointed observation on 1978 Dec 2. The phase averaged spectrum is a power law, with an energy index α of 0.1 ± 0.1 similar to that found by Becker et al. (1978). The extended energy range of HEAO-1 A2 reveals a break at ~ 18 keV above which energy the spectrum steepens with an e-folding energy of ~ 16 keV. The MED fit requires an additional soft excess with a thermal bremsstrahlung temperature of ~ 0.3 keV, 3 times lower in temperature than that reported by Becker et al. (1978). This excess may come, in part, from stars in the nearby Cyg OB2 association (cf. Harnden et al. 1980). The photo-electric absorption, kept the same for both components in the spectral fitting, is ~ 7×10^{22} H cm^{-2}.

The iron line EW is 1340±60 eV (0.014±0.003 ph cm^{-2} s^{-1}) at 6.76±0.03 keV with a FWHM of 1.0±0.1 keV, again in reasonable agreement with that seen previously (Becker et al. 1978). The χ^2 for the fits from both detectors are poor, with 335 for 36 dof and 931 for 46 dof in the MED and HED,

respectively. The residuals indicate this to be the result of poor modelling of the iron line and the high energy break. As the iron line used is a simple gaussian, more complicated line blends can be approximated with a sum of two lines, one narrow and one broad, which gave χ^2 of 107 and 330 in the MED and HED, respectively. The EWs of the narrow and broad component are 830 ± 40 and 840 ± 50 eV (0.0081 ph cm^{-2} s^{-1}) at energies of ~ 6.78 and 6.51 keV. The width of the broad component is 2.4 keV. The deconvolved spectrum, using the single line fit, is shown in Figure 11.

A sensitive model independent indicator of spectral variability across the 4.8-hr modulation is the ratio of the rate in each PHA channel obtained at maximum, to that obtained at minimum light. These are shown in the left hand side of Figure 12 for the HEAO-1 A2 data such that an increase in the depth of modulation causes the ratio to increase (i.e. more absorption at minimum light causes a larger PHA ratio at low energies). The following conclusions may be drawn from Figure 12.

1. The ratio decreases at low energies, suggesting that the soft component is modulated differently than is the higher energy component.
2. There is a dip around ~ 6.7 keV, indicating a difference in the modulation of the iron line relative to the local continuum.
3. The spectrum hardens at minimum light.

These points are essentially in good agreement with the conclusions of Becker et al. (1978). Because of the interdependence of the parameters it is difficult to quantify these variations, in particular the variations in the iron line. For a single gaussian line there is no formal statistical evidence for a change across the modulation in either the line energy or the EW. The two-component line again gives the same EW (within ~ 10%) but there is evidence that the centroid energy of the broad component had increased

to ~ 6.7 keV at minimum light, similar to the shift seen by Becker et al. (1978).

The 7 arc min field of view of the SSS (compared to ~ 3^0 for HEAO-1 A2), did not include any known sources in the Cyg OB2 association. The observation was, in part, simultaneous with the HEAO-1 A2 measurement just discussed. The ratios of the PHA rates at minimum and maximum light, shown in Figure 13, again decrease at low energies and suggest the presence of an unmodulated soft component. Formal fits to the total data set for the model of a single power law plus absorption model give an unacceptable χ^2 of 285 for 63 dof, with a large fraction of this χ^2 associated with the structure in the spectrum near ~ 2.5 keV (Figure 14). The inclusion of a soft thermal component with kT ~ 0.3 keV gives a χ^2 of 238, and the further inclusion of a broad sulfur line at ~ 2.5 keV reduces χ^2 to 101. This fit is shown in the middle trace of Figure 13, where the unmodulated soft component replicates the softening in the PHA ratio. The EW of the sulfur line relative to the continuum is 177 ± 30 eV at an energy of 2.54 ± 0.04 keV, with a width of 0.27 ± 0.05 keV. The luminosity of the soft component is a factor two below that derived from the MED data, and almost an order of magnitude below that required by Becker et al.

Even with such a small FOV there still exists the possibility that the soft component is not intrinsic to Cyg X-3, but rather comes from a contaminating star within 4 arc min (e.g. Figure 1, Harnden et al.). The temperature of ~ 0.3 keV is typical of that seen from OB stars (Swank, priv. comm.) and with ~ 50% lower column density than Cyg X-3, the luminosity is similar to the X-ray bright stars seen by Harden et al. The measured absorption for Cyg X-3 corresponds to $(7\pm3) \times 10^{22}$ H cm^{-2}, where the uncertainty includes the possibility that the soft emission is not intrinsic

to Cyg X-3.

High state spectral data were obtained from HEAO-1 A2 scanning observations made between 1977 Nov 16 and 26. The PHA ratios of the maximum to the minimum phases for the high state are also shown in Figure 12, and the most obvious difference from the low state is that the unmodulated soft excess is not apparent in the high state data. The other aspects of the variability of the ratio with energy are similar in both states, including the dip at the iron line and the tendancy for a harder spectrum at minimum. Acceptable fits to the data can be obtained with a relatively flat power law plus a steeper second component. For reasons discussed in the next section we assume that the steep component is a blackbody. The best fit gives a blackbody temperature of 1.2 ± 0.1 keV in both detectors, and α of 0.6 ± 0.1 in the MED and 0.9 ± 0.1 in the HED. The iron line EW is 575 ± 190 eV (0.039 ± 0.011 cm^{-2} s^{-1}) centered at 6.56 ± 0.15 keV, with a width of 1.3 ± 0.4 keV. The χ^2 are 75 for 36 dof, and 61 for 17 dof, for the MED and HED, respectively. These results agree with those found earlier for the high state by Blisset, Mason and Culhane (1981), except that we see no evidence for any phase related variations in the blackbody component. The deconvolved spectra for both the high and low states are shown in Figure 11.

SSS observations of the high state were made on 1979 May 9 and 10. A blackbody model gives the best simple fit, with kT ~ 1.5 keV and a χ^2 of 507 for 55 dof. The inclusion of a second continuum component does not substantially improve the fit. Sulfur and silicon lines at 2.61 and 1.6 keV, each with EWs of 40 ± 20 eV and line widths of ~ 0.2keV, do improve the fit, although not so much as to make it formally acceptable. The best fit high state column density is (3±1) x 10^{22} H cm^{-2}, in reasonable agreement with the radio measurement (Chu and Bieging 1973). The PHA ratio shows no evidence for

any increase (or decrease) at low energies. The upper limit to any phase related change in absorption is $< 1.5 \times 10^{22}$ H cm^{-2}. This takes into account any uncertainty in the underlying continuum.

For a distance of 10 kpc (Chu and Bieging 1973) the 1-60 keV luminosity is 4.4×10^{37} erg s^{-1} in the low state and 1.2×10^{38} ergs s^{-1} in the high state . All of the evidence is consistent with the additional soft component observed in the low state being external to the source. Observable in the low state only, its apparent lack of 4.8-hour modulation, in all the data available to us, suggests that its origin may lie outside Cyg X-3. If it were truly associated with Cyg X-3, and it had a blackbody spectrum for which the high energy tail is observable in the X-ray band as the soft component, this component would dominate the total source output with a luminosity in excess of 10^{39} erg s^{-1}, in this blackbody component alone. The high-state blackbody component is modulated with the 4.8-hour variation and would totally mask the presence of the soft component seen in the low state in the X-ray band.

These results can be summarized as follows:

1. Cyg X-3 shows two distinct intensity states. The low state is an $\alpha \sim 0$ power law with high energy cutoff at ~ 19 keV. In the high state the power law is steeper, $\alpha \sim 1$, and there is a second ~ 1.2 keV blackbody component.
2. No variation in absorption across the modulation is observed.
3. There is an intense 1-2 keV broad iron line at ~ 6.7 keV, with a possible slight dependence in the energy centroid of the line feature with the 4.8-hr modulation. The EW in the high state is ~ 700 eV and in the low state is ~ 1600 eV. The number of photons in the line increases from the low to high state by a factor 5.
4. There is a narrower, ~ 0.3 keV wide, sulfur line feature at ~ 2.5 keV. While the number of line photons increases from the low to high state, the EW

decreases from 177 ± 30 eV to ~ 40 ± 20 eV.

5. In the low state there is a bright ($L_x \sim 10^{39}$ ergs s^{-1} if truly associated with Cyg X-3) unmodulated soft excess (kT ~ 0.25 keV) that is not related to the blackbody component in the high state spectrum.

b) 4U1822-37

In paper 1 we found that:

1. This source is stable over many years and shows a flat, $\alpha \sim 0$, power law with a high energy cutoff at ~ 18 keV.

2. The secondry modulation is absorption independent and the column density is ~ 3 x 10^{21} H cm^{-2}.

3. An 1100 eV EW iron line is present with a FWHM of 4.4 ± 2.0 keV.

4. The spectrum contains a soft excess with a thermal temperature of ~ 0.25 keV, or a power law with an α of 4.5 ± 1.0, and a luminosity about 0.01 to 0.1 the hard component, or broad iron L-emission at ~ 1 keV with an EW of ~ 400 eV.

c) 4U2129+47

The low state data come from a HEAO-1 A2 pointed observation in Dec 1978, and the high state data are from SSS/MPC and were taken six months later.

The MED gives a power law with α = 1.1 ± 0.2 for a χ^2_r = 0.8, or a thermal of temperature 7.3 ± 1.5 keV for χ^2_r = 1.3. For both spectral models a 425 ± 250 eV EW iron line with a FWHM < 3.5 keV is required. The column density is < 5 x 10^{21} H cm^{-2}. The HED gives similar results, with a slightly better χ^2_r for the power law. The SSS spectrum, taken when the source was bright, indicates a flatter spectrum with α = 0.3 ± 0.3 or kT > 8.0 keV (χ_r = 0.8 in both cases). The MPC, however, gives α = 1.0 ± 0.1 for χ^2_r = 3.2, or kT = 8.9 ± 1.0 keV for χ^2_r = 0.7, in the 1.5 to 20 keV band. The inverted spectra

for all three detectors can be compared in Figure 14. All the data are marginally consistent with a single thermal spectrum of ~ 8 keV. The high state flux in the 0.5 to 60 keV band is 3×10^{-10} ergs $cm^{-2}s^{-1}$, which gives a luminosity of 10^{36} ergs s^{-1} for a distance of 5 kpc.

VIII. SPECTRAL INTERPRETATION

All models for Cyg X-3, 4U1822-37 and 4U2129+47 must invoke the Comptonization of photons from a central X-ray source to explain the X-ray light curves. The nature of this process in an astrophysical setting has been discussed by many authors (e.g. Illarionov and Sunyaev 1972; Felten and Rees 1972; Shapiro, Lightman and Eardley 1976; Katz 1975).

a) 4U1822-37 and Cyg X-3

The low state Cyg X-3 spectrum and the spectrum of 4U1822-37 are remarkably similar. For a scattering medium with a temperature which is well below the characteristic source temperature, the electron recoil effect will dominate the Compton scattering process, and a break will be seen in the spectrum at $E_B = M_e c^2/\tau^2$ (Illarionov and Sunyaev 1972). The high energy cutoff in 4U1822-37 and the low state of Cyg X-3 is a direct measure of the optical depth to the central X-ray object, and gives, in both cases, $\tau \sim 5$. As τ increases, the energy of the high energy cutoff will decrease, approaching the temperature of the corona. For $\tau > 10$ photons will become sufficiently thermalized to form a Wien peak with the characteristic temperature of the corona. The high state of Cyg X-3 can be reconciled with an increase in τ to $\gtrsim 10$ that may be associated with an increase in the central source luminosity. The fact that there is a high energy tail indicates a non-uniform or leaky scattering medium (which would be expected from an ADC, cf Figure 4). The blackbody spectrum gives a temperature

of ~ 1.5 keV for the scattering medium.

The fact that both 4U1822-37 and Cyg X-3 display intense broad iron line emission at 6-7 keV further emphasises that these sources may be fundamentally similar. The EWs of order 1000 eV are at least a factor 2 greater than that seen from other binary X-ray sources. An optically thick ADC provides an ideal environment for the production of line emission, either from recombination in the corona (Ross, Weaver and McCray 1978; Ross 1979; Fabian and Ross 1981), or from the fluorescence of iron at the surface of the accretion disk (paper 1). Either process must account for the factor 2 decrease in the EW during the high state of Cyg X-3. In the high state the reduced fluorescence efficiency, caused by the softer continuum above 7.1 keV, is consistent with lower EW. However, the observed EWs requires, for solar abundances, that the flux at the surface of the disk is a factor 10 larger than that seen from our line of sight (paper 1); this is unlikely for the geometry discussed in V. Recombination in the corona may be preferable to fluorescence but the predicted EWs and spectra are critically dependent on the assumed density structure of the ADC, a highly uncertain parameter for the Compton-thick case.

The broadening of the line profiles is a direct consequence of the presence of the hot Compton-thick ADC. The iron line profile, including the energy centroid, conveys information concerning both the temperature and the optical depth of the scattering medium (Sunyaev and Titarchuk, 1980, ST; Pozdnyakov, Sobol, and Sunyaev 1979, PSS). If the temperature of the corona is hotter or cooler than the line energy, the scattering will broaden the line profile and shift its centroid. The line energy and width of Cyg X-3 is the same in both the low and high states, which infers $kT_c \sim 2$ keV for τ between 5 and 10 (cf Figure 4 of ST and Figure 4 of PSS). This is in reasonable

agreement with the Wien peak temperature. The width of the line in 4U1822-37 is about a factor two larger and infers $kT_c \sim 4$ keV. All these values are consistant with the coronal temperatures inferred from the measured coronal radii.

In Paper 1 we suggested that the soft excesses from Cyg X-3 and 4U1822-37 might be free-free emission from their coronae, with a kT_c of ~ 0.25 keV. This no longer appears to be viable, as the combination of the required τ and such a low coronal temperature would cause the iron line to be measurably shifted to lower energies. A conservative estimate of the emission measure EM of the corona can be obtained by assuming the vertical density structure is constant at n_{max} and cuts off at 0.1 R_o. This gives a luminosity for the free-free emission with a temperature of a few keV about a factor 100 below that of the observed emission.

The disk acts as a partition across the center of the corona which, because it absorbs at least $\sim 30\%$ of the scatterred radiation which is then re-emitted as a far UV albedo ($kT \sim 0.01\ kT_c$), substantially amplifies (by two orders of magnitude) the number of photons in the corona. The Doppler effect will dominate the Compton scattering of the disk albedo, which cools the corona (e.g. Katz 1976; Shapiro, Lightman and Eardley 1976). The Comptonized spectrum is relatively independent of the input spectrum and for low τ it will be a power law from the disk surface temperature up to $\sim kT_c$, above which it decays as a Wien tail. The energy index α is given by ST and Shapiro, Lightman and Eardley to be

$$\alpha = \left(\frac{9}{4} + \nu\right)^{1/2} + \frac{3}{2}$$

$$\nu = \pi^2 . m_e c^2 / 3 . \left(\tau + \frac{2}{3}\right)^2 kT_c$$

An upper limit to τ can be obtained from the point at which catastrophic cooling sets in, which from ST is $\nu \lesssim 5$. This predicts τ = 8-11 for kT_c = 2-5 keV, in reasonable agreement with the observed values. The soft excess from 4U1822-37 may be the high energy tail of the albedo component. The measured α for this component of 4.5±1.0 is consistent with the predicted value of 5. Such a soft component from Cyg X-3 would be undetected because of the high column density to that source.

The X-ray spectra of 4U1822-37 and Cyg X-3 are therefore consistent with being the result of the Comptonization of a hard X-ray spectrum in a hot 10^7 K optically thick plasma, such as would be found in an ADC. Previously proposed models for Cyg X-3 cannot reproduce all the experimental details. Scattering in an optically thick stellar wind from the secondary or a shell surrounding the entire system has been proposed to account for the 4.8 hr modulation from Cyg X-3 (Davidsen and Ostriker 1974; Pringle 1974; Milgrom 1976). Elsner et al. (1980) and Ghosh et al. (1981) have considered these models in great detail and can reproduce the asymmetric light curve of Cyg X-3 with an eccentric orbit. Our data suggest the high and low state of Cyg X-3 involve changes in τ which, for the stellar wind or shell models, implies that the high state light curve should be much less modulated, in contrast to the constant fractional modulation observed (Figure 9). Further, if the scattering is in a stellar wind then an increase in absorption at minimum light, an order of magnitude larger than our upper limit of $< 1.5 \times 10^{22}$ H cm^{-2}, is to be expected. Lastly, apsidal motion will cause the light curve to change and the lack of any such change over the past 5 years constrains the secondary to be a helium star. For an ad hoc shell surrounding the system the helium star must be "dressed" to reproduce the duty cycle. There is too much

extinction to Cyg X-3 to check the nature of the secondary directly. For 4U1822-37, however, a helium star cannot be reconciled with the observations.

b) 4U2129+47

The relatively soft ~ 8 keV thermal character of the spectrum of 4U2129+47 is very reminiscent of that seen from the Sco X-1/galactic bulge sources (e.g. Mason et al. 1976). In these sources deviations, from a pure bremsstrahlung model have been accounted for by Comptonization in an optically thick X-ray emitting plasma (e.g. Lamb and Sanford 1979). The ADC model provides a natural environment for such a process to occur, and 4U2129+47 may provide the key to understanding these enigmatic sources. The spectrum of 4U2129+47 probably differs from that of 4U1822-37 and Cyg X-3 because of a generic difference in the nature of the central X-ray emitting region. For example the magnetic field on the accreting neutron star may be weak and allows the accretion disk to penetrate close to the neutron star surface. Because of this the optical depth of the corona in the central region may be very high, in which case the radiative transfer is dominated by bremsstrahlung losses from the corona itself (Fabian, priv. comm.).

IX LUMINOSITIES

A possible distinguishing property between turbulent and evaporated coronae is the source luminosity, i.e. an evaporated Compton thick corona should not be found in a source with $L_X \lesssim 10^{37}$ ergs s^{-1}. The observed scattered luminosity L_{obs} will be lower than the true source luminosity L by the fractional solid angle subtended by the corona, sin $\theta_{\tau=1}$ (where $\theta_{\tau=1}$ is the angle above the disk plane at which $\tau = 1$). From Figure 3 $\theta_{\tau=1} \gtrsim 45^{o}$, so $L_{obs} \sim 0.7$ L. This gives an average high state luminosity for Cyg X-3 comparable to the Eddington limit for 1.4 M_{o} star, which suggests that this source contains an evaporated corona.

4U1822-37 is at $\ell = 357^{o}$ and $b = -11^{o}$, and only a lower limit to its distance of 500 pc exists (Mason et al. 1980). If its luminosity is similar to the low state Cyg X-3 value then its distance is $\gtrsim$ 10 kpc and the source is a halo object somewhere on the other side of the galaxy (Paper 1). Recently Cowley, Crampton and Hutchings (1982) have reported that 4U1822-37 has peculiarly large space motion of -90 km s^{-1}. This supports the idea that this source is in the galactic halo.

The distance to 4U2129+47 is estimated to be between 2-5 kpc (McClintock, Remillard and Margon 1981), so that $L \lesssim 10^{36}$ ergs s^{-1}, which is too low for a Compton thick evaporated corona. Rather than invoking mechanical heating of the corona for 4U2129+47, it is possible that because the inclination of this system is $> 82^{o}$, the central area of the disk and a large part of the corona are hidden behind the disk rim (analogous to a permanently turned off Her X-1). This may also explain why the optical light curve of 4U2129+47 is dominated by the X-ray-heated secondary, and not, as is the case for 4U1822-37, the light from the accretion disk. Therefore all three sources may well contain <u>evaporated</u> ADC.

X. SUMMARY AND CONCLUSION

The principle results can be summarized as follows:

1) The X-ray emission from 4U2129+47 is diffused by an ADC and the X-ray source appears to be extended with a radius of $\sim 0.6\ R_{o}$, compared to $\sim 0.3\ R_{o}$ for 4U1822-37.

2) ADC are probably generated by the evaporation of hot material from the surface of the accretion disk by the central X-ray source. An evaporated ADC will only become optically thick when L_{x} approaches the Eddington limit of a 1.4 M_{o} neutron star.

3) Secondary modulations of the light curves of 4U1822-37 and 4U2129+47 can

be understood as the partial occultation of the ADC by structure in the outer regions of the accretion disk arising from turbulence induced by the inflowing gas stream.

4) Detailed modelling of the light curve of 4U1822-37 indicates two major structures in the outer disk thickness, one at the initial point of impact of the gas stream with the disk and a second $\sim 230^{o}$ around from that point.

5) This model can be extended to account for the 4.8 hr modulation of Cyg X-3. In this case the inclination is such that the eclipse by the companion is not seen.

6) The X-ray spectra of Cyg X-3 and 4U1822-37 are very similar and can be qualitatively understood as resulting from the Comptonization of a hard X-ray spectrum by an optically thick ADC.

7) We set an upper limit to any phase related changes in absorption from Cyg X-3 of $< 1.5 \times 10^{22}$ H cm^{-2}.

8) The spectrum of 4U2129+47 is similar to that from the Sco X-1/galactic bulge sources and indicates that the central X-ray source in this system is different from that in 4U1822-37 and Cyg X-3.

9) The inclinations of Cyg X-3, 4U1822-37 and 4U2129+47 are $\lesssim 70^{o}$, $\sim 75^{o}$ and $\gtrsim 82^{o}$ respectively. The X-ray heated central region of the accretion disk of 4U2129+47 is probably hidden behind a thick rim around the periphery of the disk.

The gamma ray emission from Cyg X-3 has often been cited as evidence for a young pulsar in this system (e.g. Milgrom and Pines 1978). The ADC model does not specifically require an accreting neutron star behind the corona, however models for the gamma ray emission that invoke inverse Compton scattering of the X-ray emission on relativistic electrons can also be accommodated in an ADC format (Meszaros, Meyer and Pringle 1977; Fabian,

Blandford and Hatchett 1977). Intense infrared emission from Cyg X-3 is also, on occasions, modulated with the 4.8-hr X-ray period with a similar light curve, but of lower amplitude (Mason et al. 1976a). This suggests that the modulated IR emission comes from the ADC. The nature of this IR flux and the dramatic radio outbursts remains puzzling.

Evaporated optically thick ADCs will only be found among the more luminous X-ray sources that are close to being Eddington-limited, which suggests that many of the bright galactic center sources may contain ADCs. Our conclusions provide independent justification for the Comptonization models which have been applied to these sources. Milgrom (1978) has suggested that the lack of eclipses in the galactic center sources is caused by a thick accretion disk shadowing the companion in these systems. Our modelling of accretion disks thickened by turbulence supports this idea, although the presence of ADCs will, in a few systems, cause partial eclipses either by the companion or the outer disk structure to be seen. These may, however, be among the fainter galactic center sources, because a large part of the corona could be hidden by the edge of the disk (similar to the situation that may exist in 4U2129+47). The recent detection of periodic absorption events from 4U1915-05 (White and Swank 1982; Walter et al. 1982), which can be understood as occultations of a central point source by structure in outer regions of the disk similar to that found here, supports the above scenario. In this case the steady luminosity of the source is $\sim 10^{37}$ ergs s^{-1}, which is below the threshold for the formation of an optically thick ADC. 4U1822-37, Cyg X-3 and 4U2129+47 may represent the "missing link" in our understanding of the bright galactic center sources and their relation to the better-understood pulsating binary X-ray sources. Future investigations into both Compton scattering processes and the dynamics of disk accretion should concentrate on reproducing

the properties of these three systems.

ACKNOWLEDGMENTS

We thank: Jean Swank and A. Fabian for discussions; E. Boldt, P. Serlemitsos, F. Marshall, R. Mushotzky, S. Pravdo, and R. Becker for their indirect contributions; R. London for a useful discussion concerning the physics of the evaporation process; J. Grindlay for the spectral analysis of the MPC data on 4U2129+47; R. Harnden for discussions concerning the contribution of the Cyg OB2 stars to the Cyg X-3 spectra; and the participants of the 1981 UCSC workshop on "Cataclysmic Variables and Related Systems" for many stimulating talks and discussions.

TABLE OPTIMUM BULGE PROFILE FITS

	(a) 4U1822-37	(b) Cyg X-3
δ	$= 40^{o} \pm 2$	40^{o} (F)
θ_D	$= 190^{o} \pm 15$	$100^{o} \pm 10$
θ_p	$= 235^{c} \pm 20^{o}$	$290^{o} \pm 15$
θ_{D2}	$= 210^{o} \pm 20$	$160^{o} \pm 15$
H_p	$= 0.55 \pm 0.05$	0.55(F)

All uncertainties are from eye estimates. (F) indicates the parameter was fixed. H_p is the height of the secondary bulge relative to the primary.

REFERENCES

Alpar, M.A. 1979, MNRAS 189, 305.

Bai, T. 1980, Ap. J. 239, 328.

Bath, G.T., Evans, W.D., Papaloizan, J., and Pringle, J.E. 1974, MNRAS 169, 447.

Becker, R.H., Boldt, E.A., Holt, S.S., Pravdo, S.H., Rothschild, R.E., Serlemitsos, P.J., Smith, B.W., and Swank, J.H. 1977, Ap. J. 214, 879.

Becker, R.H., Rothschild, R.E., Boldt, E.A., Holt, S.S., Pravdo, S.H., Serlemitsos, P.J., and Swank, J.H. 1978, Ap. J. 209, L65.

Bisnovatyi-Kogan, G.S. and Blinnikov, S.I. 1977, Astr Ap 59, 111.

Blissett, R.J., Mason, K.O., and Culhane, J.L. 1981, MNRAS 194, 77.

Bonnet-Bidaud, J.M. and van der Klis, M. 1981, Astr. Ap. 101, 299.

Chester, T.J. 1979, Ap. J. 230, 107.

Chu, K.W. and Bieging, J.H. 1973, Ap. J. 179, L21.

Cowley, A.P., Crampton, D., and Hutchings, J.B. 1982, preprint.

Davidsen, A. and Ostriker, J.P. 1974, Ap. J. 189, 331.

Elsner, R.F., Ghosh, P., Darbo, W., Weisskopf, M.C., Sutherland, P.G., and Grindlay, J.E. 1980, Ap. J. 239, 335.

Fabian, A.C., Blandford, R.D., and Hatchett, S. 1977, Nature 266, 512.

Fabian, A.C. and Pringle, J.E. 1978, MNRAS 180, 749.

Fabian, A.C. and Ross, R.R. 1981, MNRAS 195, 29p.

Felten, J.E. and Rees, M.J. 1972, Astr Ap 17, 226.

Flannery, B.P. 1975, MNRAS 170, 325.

Galeev, A.A., Rosner, R. and Vaiana, G.S. 1979, Ap. J. 229, 318.

Ghosh, P., Elsner, R.F., Weisskopf, M.C., and Sutherland, P.G. 1980, preprint.

Ghosh, P. and Lamb, F.K. 1979, Ap. J. 234, 296.

Harnden, F.R., Branduardi, G., Elvis, M., Gorenstein, P., Grindlay , J., Pye,

J.P., Rosner, R., Topka, K., and Vaiana, G.S. 1979, Ap. J. 234, L51.

Hassall, B.J.M., Pringle, J.E., Ward, M.J., Whelan, J.A.J., Mayo, S.K., Echevarria, J., Jones, D.H.P., and Wallis, R.E. 1981, MNRAS 197, 275.

Icke, V. 1976, in proc. IAU Symp. 73, The Structure and Evolution of Close Binary Systems, ed. P. Eggleton, S. Milton and J. Whelan (Dordrecht:Reidel), 267.

Illarionov, A.F. and Sunyaev, R.A. 1972, Sov. Astron.-AJ 16, 45.

Jones, C. and Foreman, W. 1976, Ap. J. 209, L131.

Katz, J.I. 1976, Ap. J. 206, 910.

Lamb, P., and Sanford, P.W. 1979, MNRAS 188, 555.

Liang, E.P.T. and Price, R.H. 1977, Ap. J. 218, 247.

Livio, M. and Shaviv, G. 1977, Astr Ap 55, 95.

Landon, R., McCray, R., Auer, L.M. 1981, Ap. J. 243, 970.

Longmore, A.J., Lee, T.J., Allen, D.A. and Adams, D.J. 1981, MNRAS 195, 825.

Lubow, S.M. and Shu, F.M. 1975, Ap. J. 198, 383.

Lubow, S.M. and Shu, F.M. 1976, Ap. J. 207, L53.

Lynden-Bell 1969, Nature 223, 690.

Mason, K.O. et al. 1976a, Ap. J. 207, 78.

Mason, K.O., Charles, P.A., White, N.E., Culhane, J., Sanford, P., and Strong K. 1976b, MNRAS 177, 513.

Mason, K.O., and Cordova, F. 1982, Ap. J., in press.

Mason, K.O., Middleditch, J., Nelson, J.E., White, N.E., Seitzer, P., Tuohy, I.R., Parkes, G.E., Murdin, P.G., and Hunt, L. 1980, Ap. J. 242, L109.

McClintock, J.E., Remillard, R.A., and Margon, B. 1981, Ap. J. 243, 900.

McCray, R. and Hatchett, S. 1975, Ap. J. 199, 196.

Meszaros, P., Meyer, F., Pringle, J.E. 1977, Nature 268, 420.

Milgrom, M. 1976, Astr Ap 51, 215.

Milgrom, M. 1978, Astr Ap 67, L25.

Paczynski, B. 1971, Ann. rev. Astron. Astrophys 9, 183.

Parmar, A.N., Sanford, P.W., and Fabian, A.C. 1980, MNRAS 192, 311.

Parsignault, D.R., Grindlay, J., Gursky, H., and Tucker, W. 1977, Ap. J. 218, 232.

Pozdnyakov, L.A., Sobol, I.M., Sunyaev, R.A. 1979, Astr Ap 75, 214 (PSS).

Pravdo, S.H., Boldt, E.A., Holt, S.S., Rothschild, R.E., and Serlemitsos, P.J. 1978, Ap. J. 225, L53.

Pringle, J.E. 1974, Nature 247, 21.

Robinson, E.L. 1976, Ann. Rev. Astron. Astrophys 14, 119.

Ross, R. R. 1979, Ap. J. 233, 334.

Ross, R.R., Weaver, R., and McCray, R. 1978, Ap. J. 219, 292.

Sanford, P.W., Mason, K.O., and Ives, J. 1975, MNRAS 173, 9.

Serlemitsos, P.J., Boldt, E.A., Holt, S.S., Rothschild, R.E., and Saba, J.L.R. 1975, Ap. J. 201, L9.

Shakura, N.I. and Sunyaev, R.A. 1973, Astr Ap 24, 337.

Shakura, N.I., Sunyaev, R.A., and Zilitinkevich, S.S. 1978, Astr Ap 62, 179.

Shapiro, S.L., Lightman, A.P., and Eardley, D.M. 1976, Ap. J. 204, 187.

Smak, J. 1979, Acta Astr 29, 825.

Sulkanen, M.E., Brasure, L.W., and Patterson, J. 1981, Ap. J. 244, 579.

Sunyaev, R.A. and Titarchuk, L.G. 1980, Astr Ap. 86, 121 (ST).

Tayler, R.J. 1980, MNRAS 191, 135.

Thorstensen, J., Charles, P.A., Bowyer, A., Briel, U.G., Doxsey, R.E., Griffiths, R.E., and Schwartz, D.A. 1979, Ap. J. 233, L57.

Ulmer, M.P. et al. 1980, Ap. J. 235, L159.

van der Klis, M. and Bonnet-Bidaud, J.M. 1981, Astr Ap 95, L5.

Walter, F. , Bowyer, S., Clarke, J.T., Mason, K.O., Henry, J.P., Halpern, J.,

and Grindlay, J. 1982, Ap. J., in press.

White, N.E., Becker, R.H., Boldt, E.A., Holt, S.S., Serlemitsos, P.J. and Swank, J.H. 1981, Ap. J. 247, 994.

White, N.E. and Swank, J.H. 1982, Ap. J., in press.

Zapolsky, H.S., and Salpeter, E.E. 1969, Ap. J. 158, 809.

FIGURE CAPTIONS

Figure 1 - The HEAO-1 A2 scanning data (with background subtracted) from 4U2129+47 folded at the optical period, with phase zero corresponding to optical minimum. The data is repeated for half a cycle.

Figure 2 - The SSS/MPC observation of 4U2129+47 folded at the optical period. The background has been removed and the plot repeated for half a cycle.

Figure 3 - The optical depth through the corona as a function of viewing inclination for various source luminosities, under the idealized condition that the radiation pressure is zero. When $\tau > 1$ the source luminosity must be scaled down (by a factor we have not attempted to calculate here) in order to account for the enhanced photon density in the corona (Ross 1979).

Figure 4 - Two idealized views of the possible appearance of the 4U1822-37 system. The cross sectional view of the disk assumes we are viewing at $\phi \sim 0.15$. The hatched and dotted areas represent the optically thick and thin regions of the ADC, respectively. The binary phases are indicated for the top view.

Figure 5 - Geometrical restrictions from the X-ray eclipses of 4U1822-37 and 4U2129+47 with T_7 set to 5 and 2, respectively. The area of uncertainty for 4U1822-37 contains both the statistical errors and the uncertainty in the mass of the neutron star. For 4U2129+47 only the statistical errors are included, and the uncertainty in the mass of the compact object will move the uncertainty region to the left or right by the indicated amount. An additional uncertainty has been considered for 4U1822-37 that pertains to the discussion of the possibility that there

is a thickening of the accretion disk at the edge caused by the inflowing material. The dashed lines give the region of uncertainty assuming that the disk thickness is much less than the coronal height. An accretion disk with appropriate "bulges" to generate the azimuthal profile for 4U1822-37 discussed in section V is indicated by the solid lines.

Figure 6 - Four predicted light curve for the eclipse of an ADC by a bulge at the edge of the disk that illustrate the effect of changing the radius of the ADC R_c for a constant disk radius R_d. The assumed bulge profile is shown at the bottom of the figure. The secondary eclipse has been excluded and the 4U1822-37 data shown for reference.

Figure 7 - The same as Figure 6 with the addition of a second bulge.

Figure 8 - Top two panels: the best fit to the HEAO-1 A2 4U1822-37 light curve for the indicated bulge profiles. Third panel down: the same fit given in the second panel down compared to an Einstein MPC observation one year later. Bottom panel: the predicted optical light curve compared to the observations from Mason et al. The dashed line represents the predicted eclipse assuming a uniformly illuminated disk interior and bulge. The solid line includes 40% of the light from a companion modulated by 100%, with minimum centered on the X-ray eclipse to approximate the effects of an X-ray heated companion.

Figure 9 - The best fit eclipse profile for Cyg X-3 in its low state compared to Einstein MPC data (top panel). In the bottom panel the fit from the low state is compared to scanning data obtained in the high state. In both cases it is assumed that the inclination is too low for the eclipse by the companion to be seen.

Figure 10 - Right panel: the allowed region for the companion radius for Cyg X-3 as a function of inclination for $M_x = 1.4\ M_\odot$, deduced from the

lack of an eclipse. Left panel: the peak height of the bulge as a function of inclination for both Cyg X-3 and 4U1822-37.

Figure 11 - The deconvolved spectrum of Cyg X-3 for its low and high states.

Figure 12 - The PHA data from the minimum and maximum of the 4.8 hr cycle presented in the form of a ratio of the former to the latter.

Figure 13 - Top Panel: the SSS PHA ratio defined in a way similar to that of Figure 12. Middle panel: the deconvolved spectrum for the two-component-plus-sulfur-line fit. The dashed line indicates the fit without the contribution from the soft component. Bottom panel: the best fit for a featureless power-law-plus-absorption model.

Figure 14 - The deconvolved spectra of 4U2129+47 for both the high and low states.

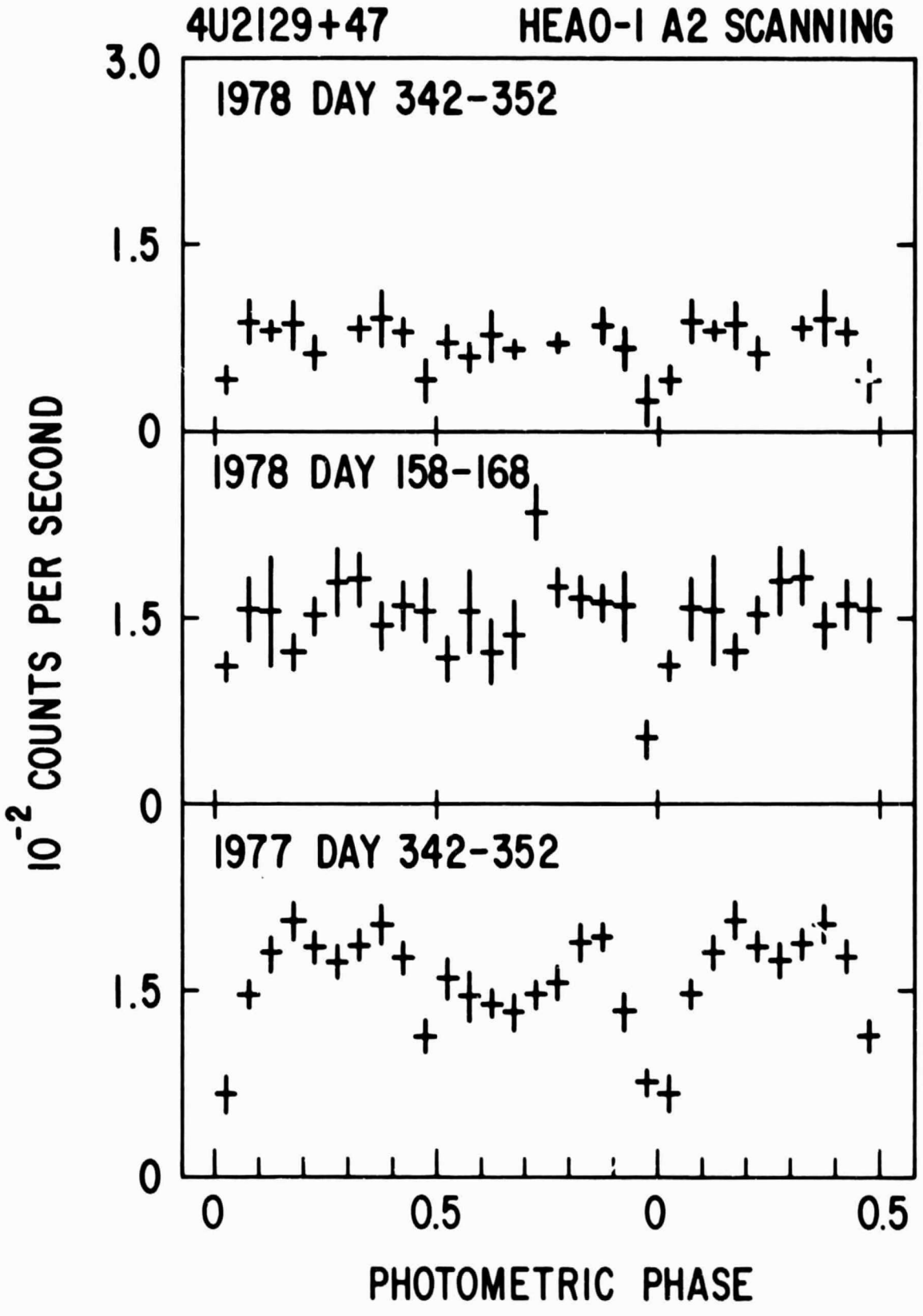
4U2129+47
HEAO-1 A2 SCANNING
1978 DAY 342-352
1978 DAY 158-168
1977 DAY 342-352
3.0
1.5
0
1.5
0
1.5
0
0
0.5
0
0.5
10^{-2} COUNTS PER SECOND
PHOTOMETRIC PHASE

Figure 1

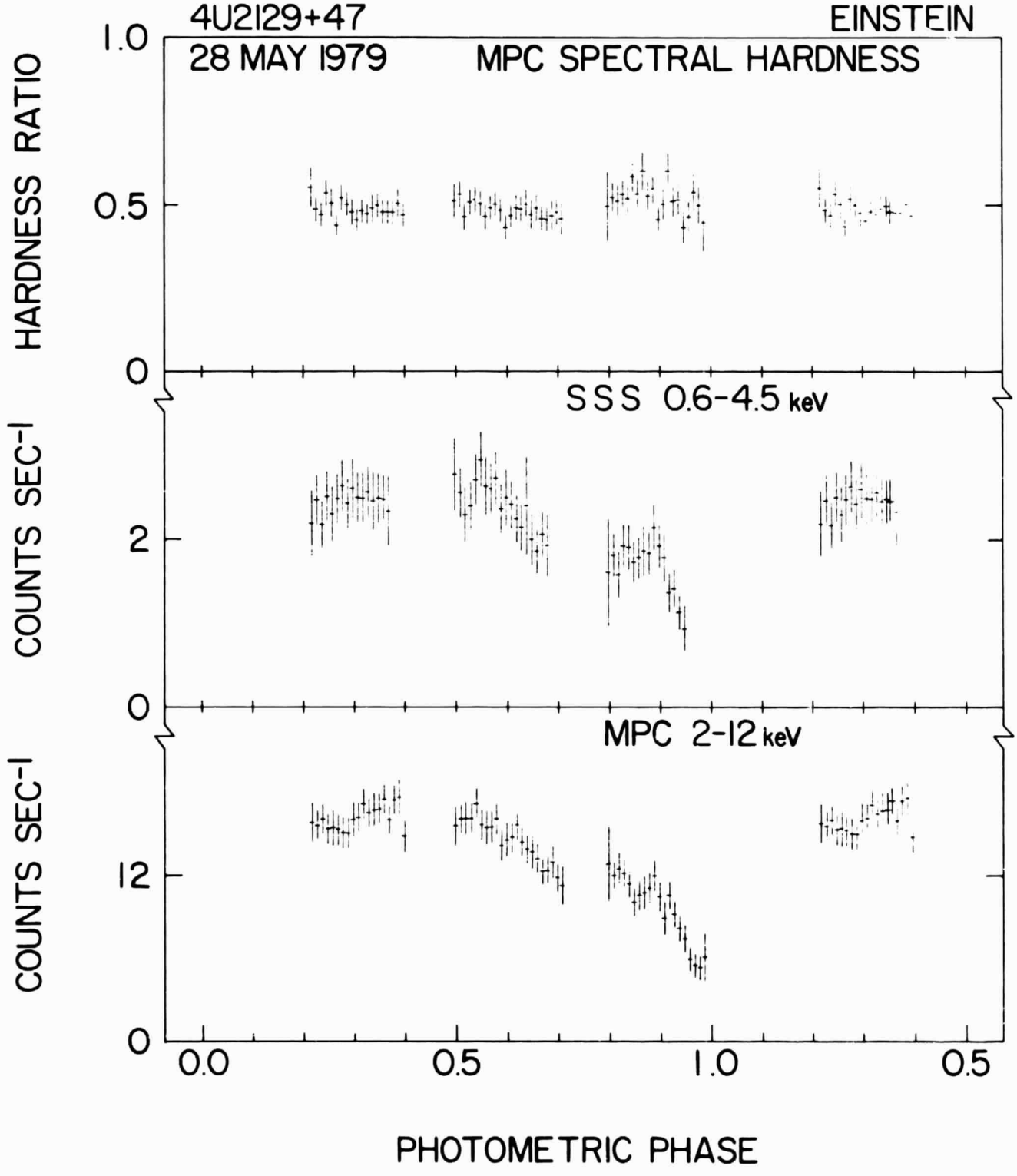
4U2129+47
EINSTEIN
28 MAY 1979
MPC SPECTRAL HARDNESS
1.0
0.5
0
HARDNESS RATIO
SSS 0.6-4.5 keV
2
0
COUNTS SEC-1
MPC 2-12 keV
12
0
COUNTS SEC-1
0.0
0.5
1.0
0.5
PHOTOMETRIC PHASE

Figure 2

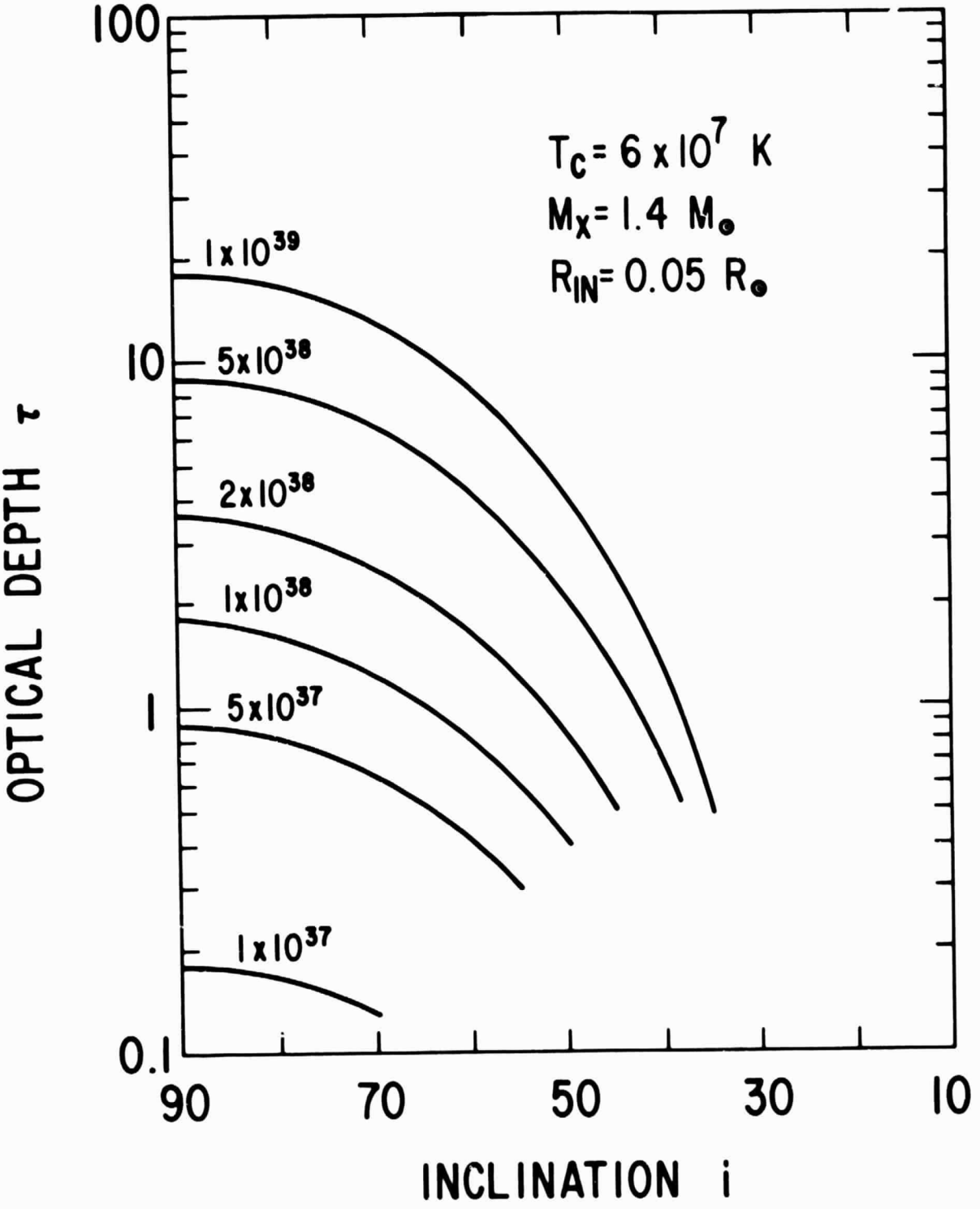
100
10
1
0.1
OPTICAL DEPTH τ
$T_C = 6 \times 10^7$ K
$M_X = 1.4\ M_\odot$
$R_{IN} = 0.05\ R_\odot$
1×10^{39}
5×10^{38}
2×10^{38}
1×10^{38}
5×10^{37}
1×10^{37}
90
70
50
30
10
INCLINATION i

Figure 3

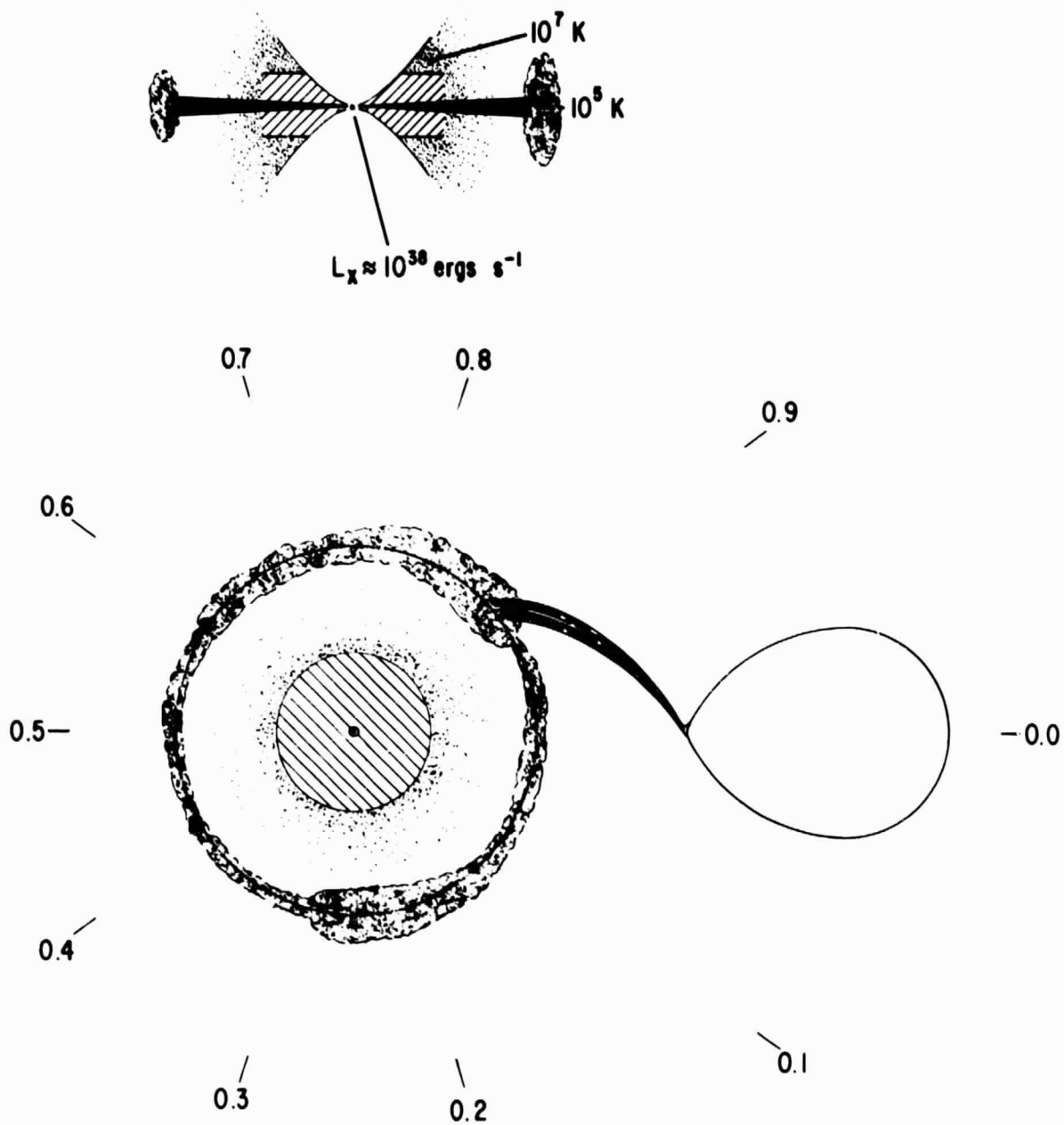

Figure 4

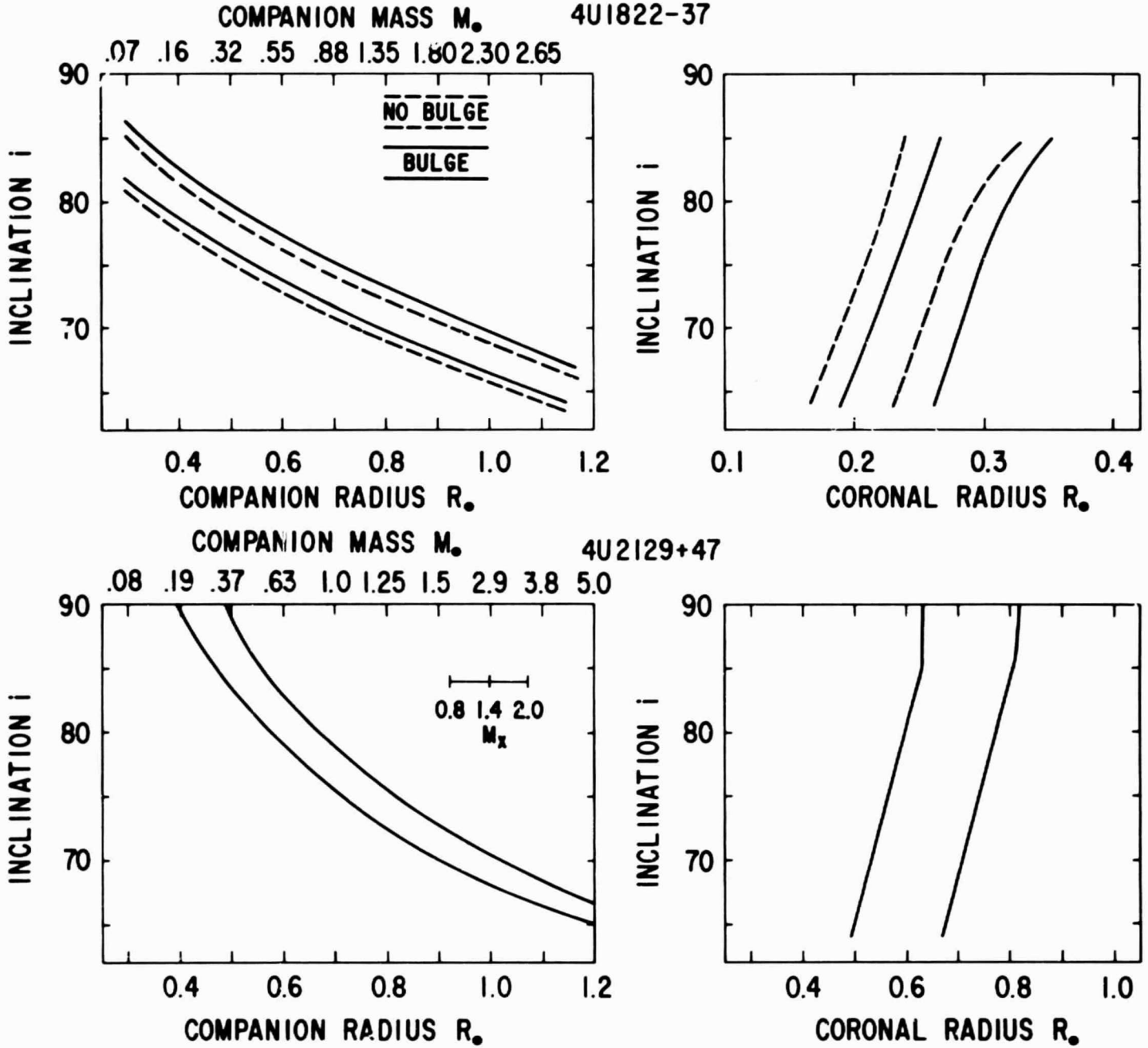
COMPANION MASS M⊙
4U1822-37
.07 .16 .32 .55 .88 1.35 1.80 2.30 2.65
NO BULGE
BULGE
INCLINATION i
90
80
70
0.4 0.6 0.8 1.0 1.2
COMPANION RADIUS R⊙
0.1 0.2 0.3 0.4
CORONAL RADIUS R⊙
COMPANION MASS M⊙
4U2129+47
.08 .19 .37 .63 1.0 1.25 1.5 2.9 3.8 5.0
0.8 1.4 2.0
M⊙
0.4 0.6 0.8 1.0

Figure 5

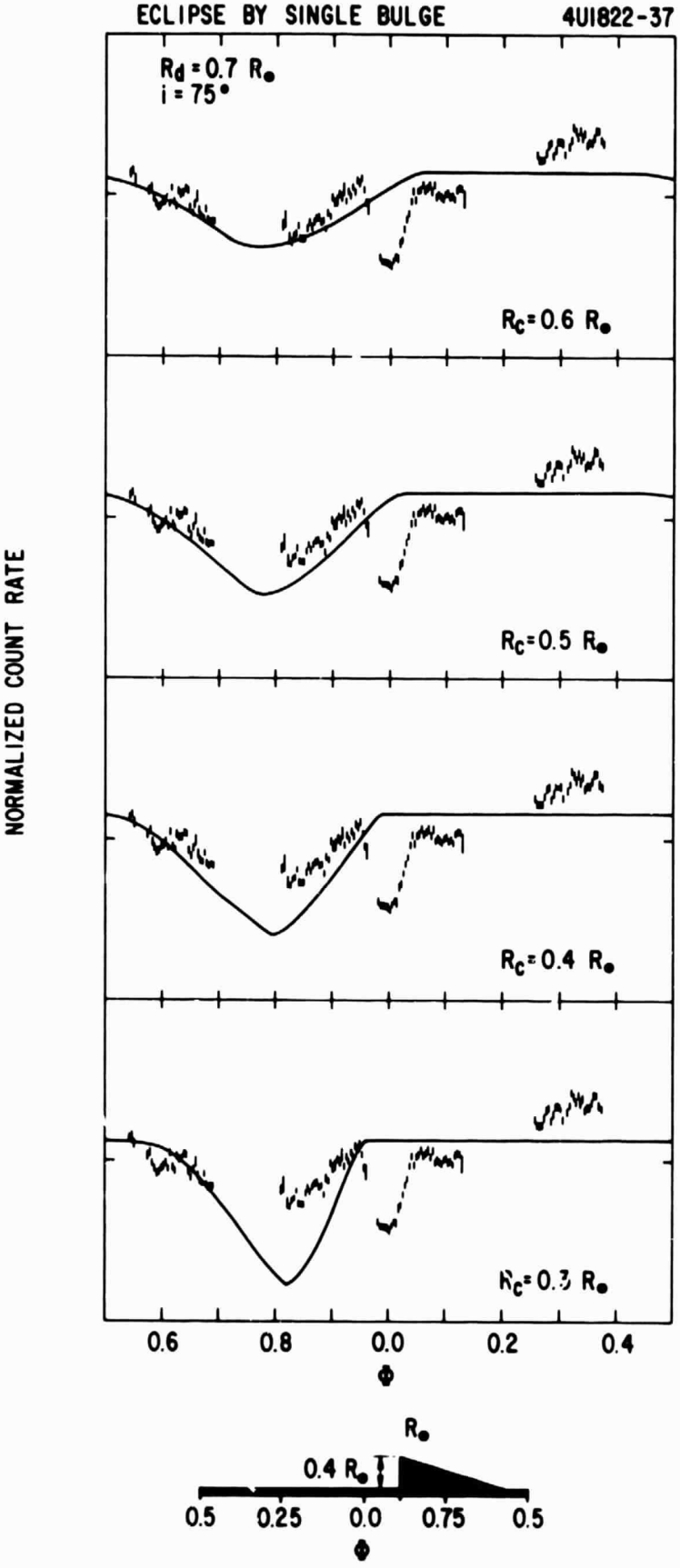
ECLIPSE BY SINGLE BULGE
4U1822-37
$R_d = 0.7\ R_\odot$
$i = 75°$
$R_c = 0.6\ R_\odot$
$R_c = 0.5\ R_\odot$
$R_c = 0.4\ R_\odot$
$R_c = 0.3\ R_\odot$
NORMALIZED COUNT RATE
0.6
0.8
0.0
0.2
0.4
Φ
$R_\odot$
$0.4\ R_\odot$
0.5
0.25
0.0
0.75
0.5
Φ

Figure 6

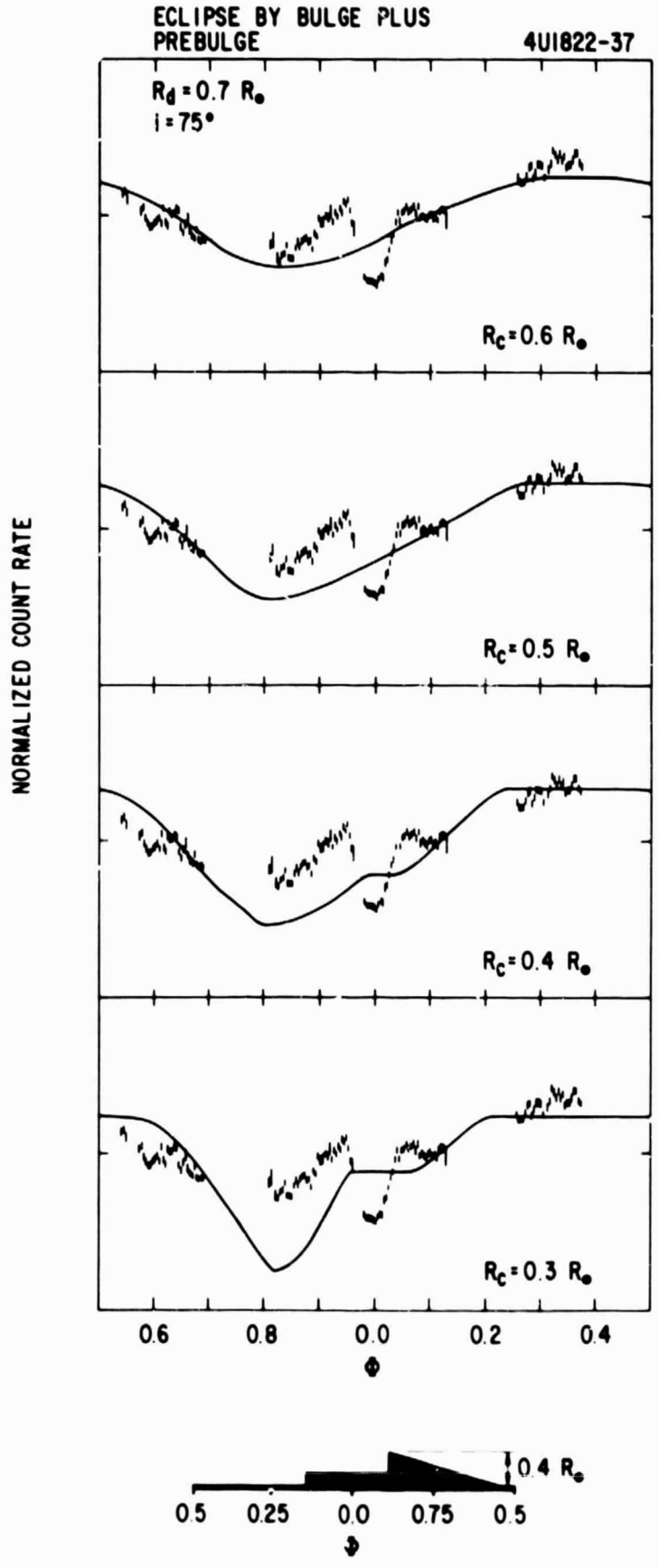
ECLIPSE BY BULGE PLUS PREBULGE
4U1822-37
$R_d = 0.7\ R_\odot$
i = 75°
$R_c = 0.6\ R_\odot$
$R_c = 0.5\ R_\odot$
$R_c = 0.4\ R_\odot$
$R_c = 0.3\ R_\odot$
NORMALIZED COUNT RATE
0.6
0.8
0.0
0.2
0.4
Φ
0.4 $R_\odot$
0.5
0.25
0.0
0.75
0.5
Φ

Figure 7

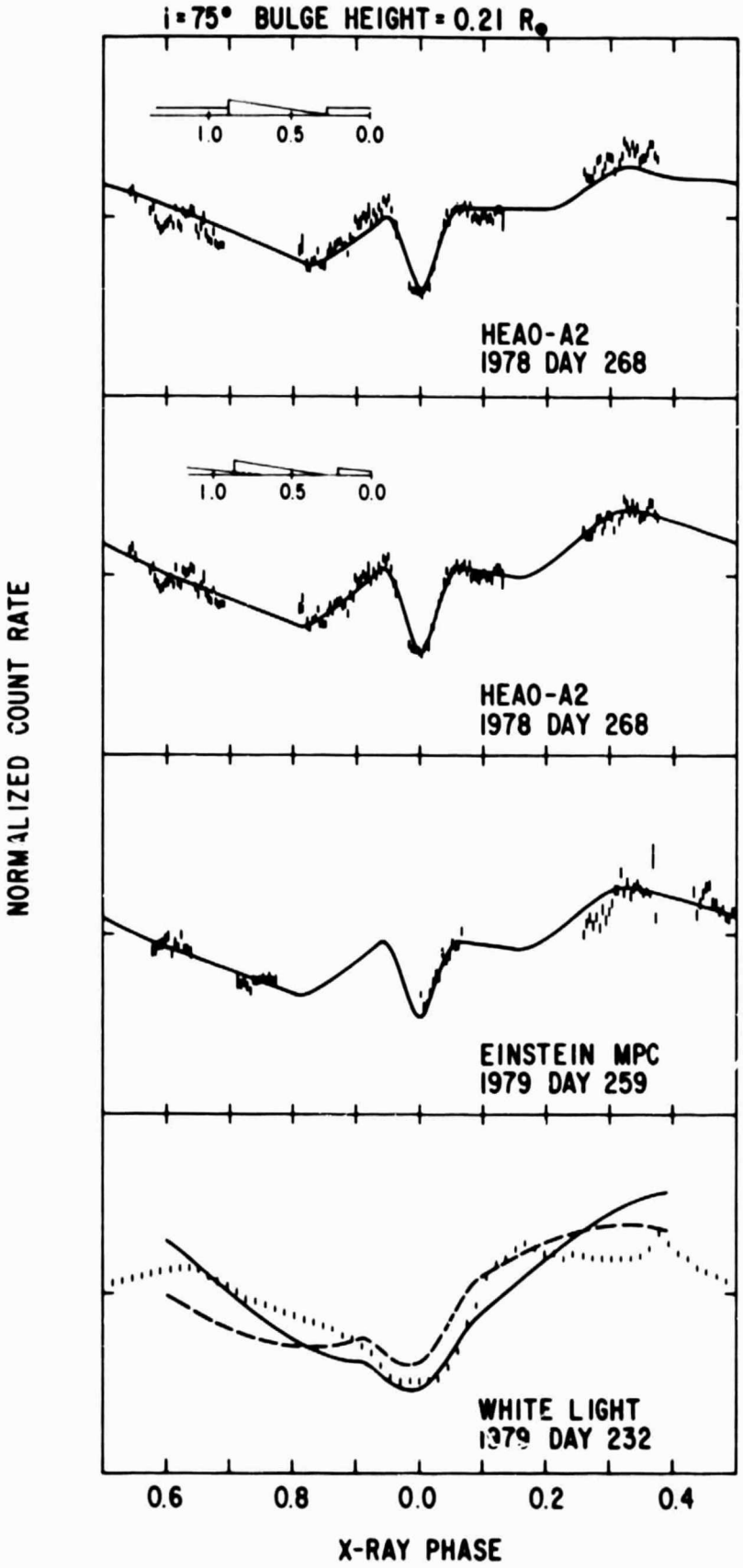
i = 75° BULGE HEIGHT = 0.21 R⊙
1.0
0.5
0.0
HEAO-A2
1978 DAY 268
1.0
0.5
0.0
HEAO-A2
1978 DAY 268
EINSTEIN MPC
1979 DAY 259
WHITE LIGHT
1979 DAY 232
NORMALIZED COUNT RATE
0.6
0.8
0.0
0.2
0.4
X-RAY PHASE

Figure 8

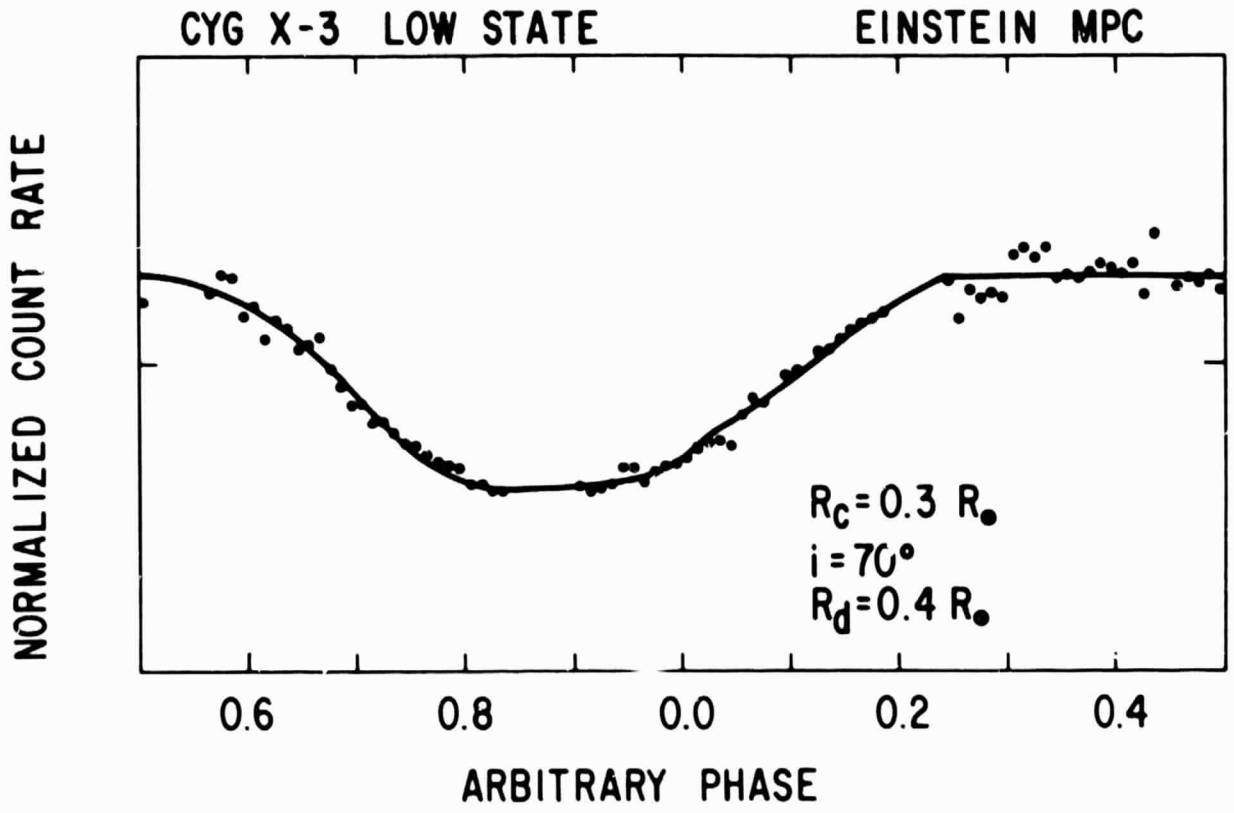
CYG X-3 LOW STATE
EINSTEIN MPC
NORMALIZED COUNT RATE
$R_c = 0.3\ R_\odot$
$i = 70°$
$R_d = 0.4\ R_\odot$
0.6
0.8
0.0
0.2
0.4
ARBITRARY PHASE

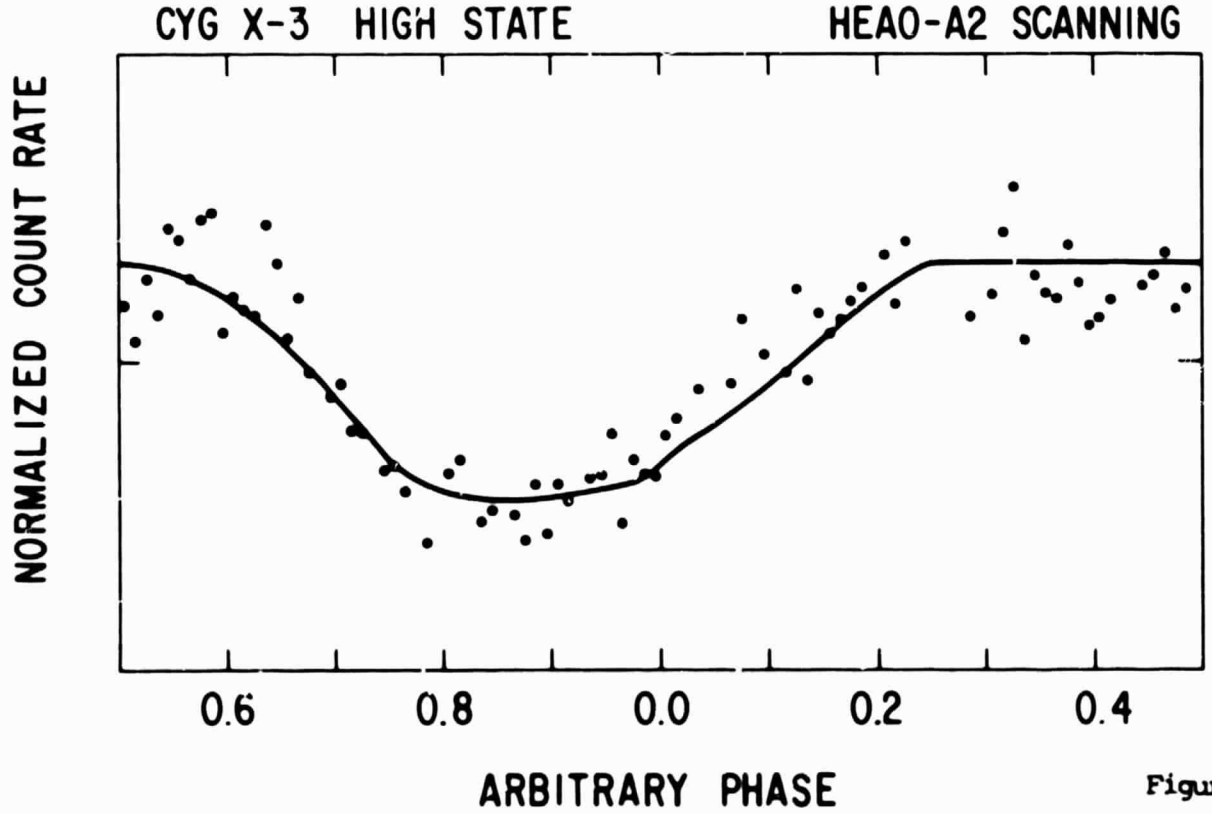
CYG X-3 HIGH STATE
HEAO-A2 SCANNING
NORMALIZED COUNT RATE
0.6
0.8
0.0
0.2
0.4
ARBITRARY PHASE

Figure 9

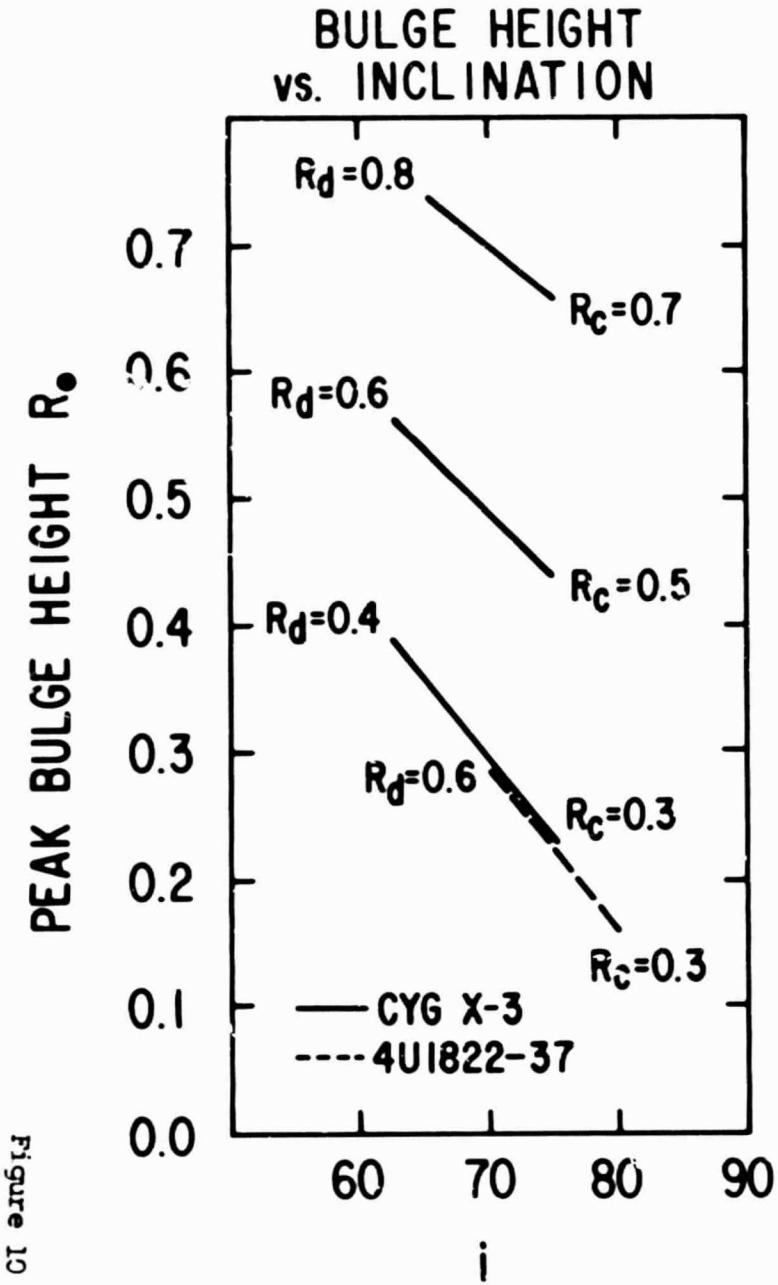
BULGE HEIGHT
vs. INCLINATION
PEAK BULGE HEIGHT R•
0.7
0.6
0.5
0.4
0.3
0.2
0.1
0.0
Rd=0.8
Rc=0.7
Rd=0.6
Rc=0.5
Rd=0.4
Rd=0.6
Rc=0.3
Rc=0.3
CYG X-3
4U1822-37
60
70
80
90
i

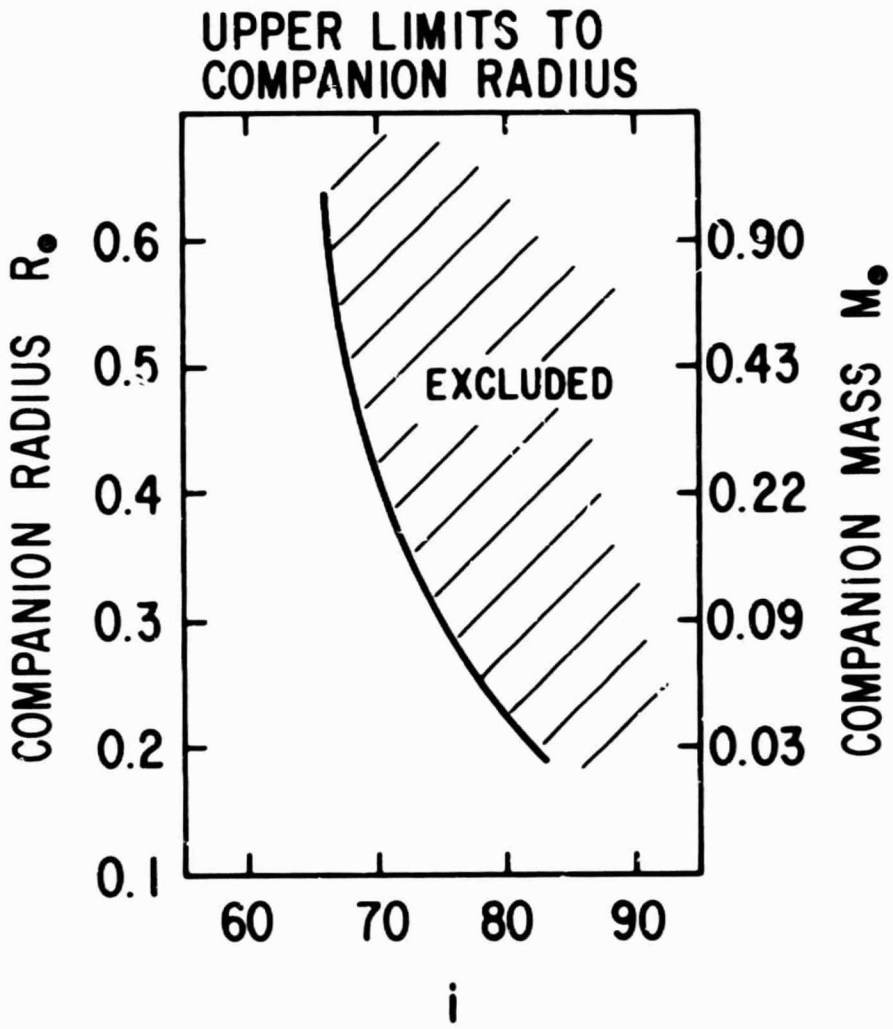
UPPER LIMITS TO
COMPANION RADIUS
COMPANION RADIUS R•
0.6
0.5
0.4
0.3
0.2
0.1
EXCLUDED
0.90
0.43
0.22
0.09
0.03
COMPANION MASS M•
60
70
80
90
i

Figure 13

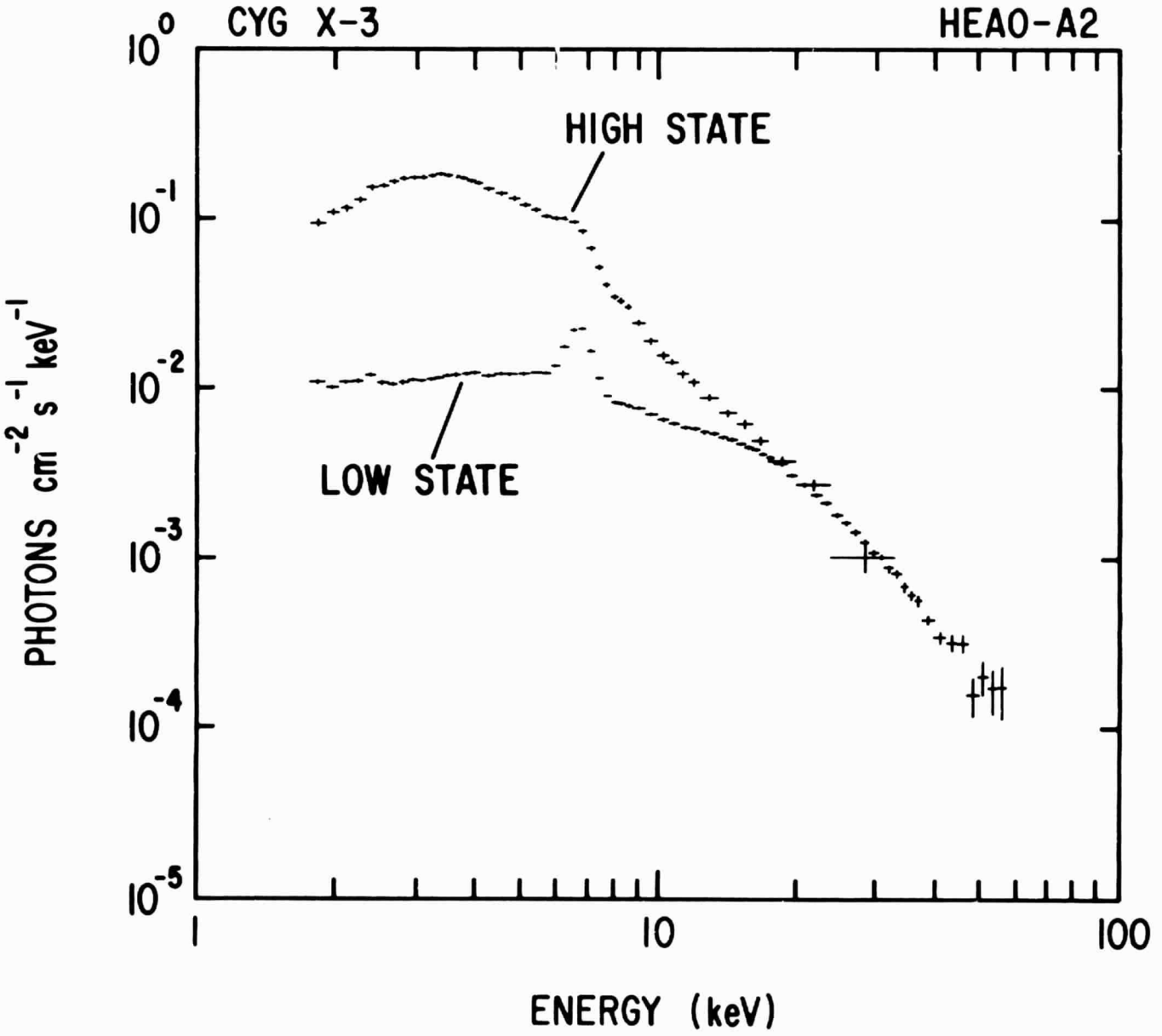
CYG X-3
HEAO-A2
HIGH STATE
LOW STATE
PHOTONS cm^{-2} s^{-1} keV^{-1}
10^{0}
10^{-1}
10^{-2}
10^{-3}
10^{-4}
10^{-5}
1
10
100
ENERGY (keV)

Figure 11

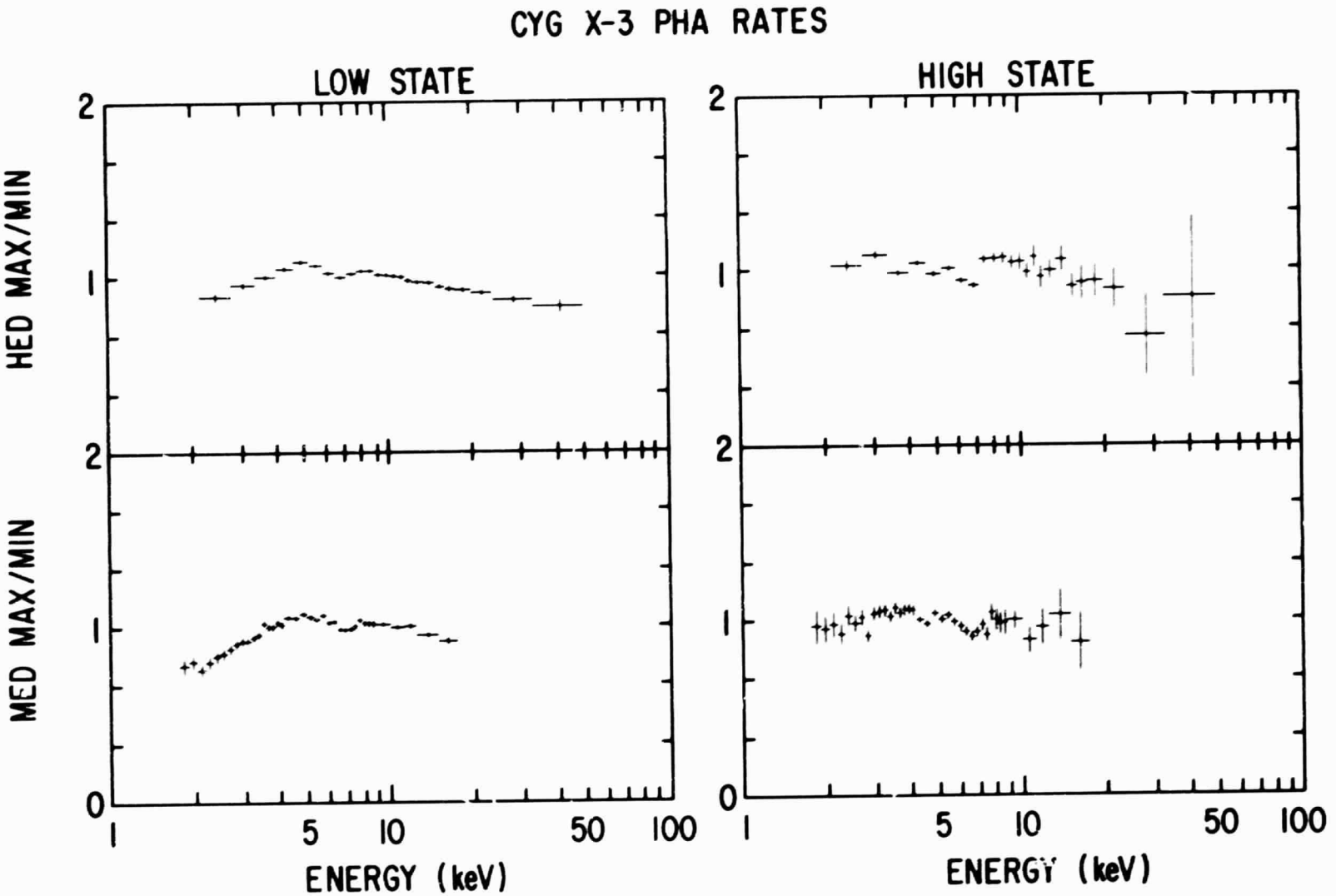
CYG X-3 PHA RATES
LOW STATE
HIGH STATE
HED MAX/MIN
MED MAX/MIN
2
1
0
1
5
10
50
100
ENERGY (keV)

Figure 12

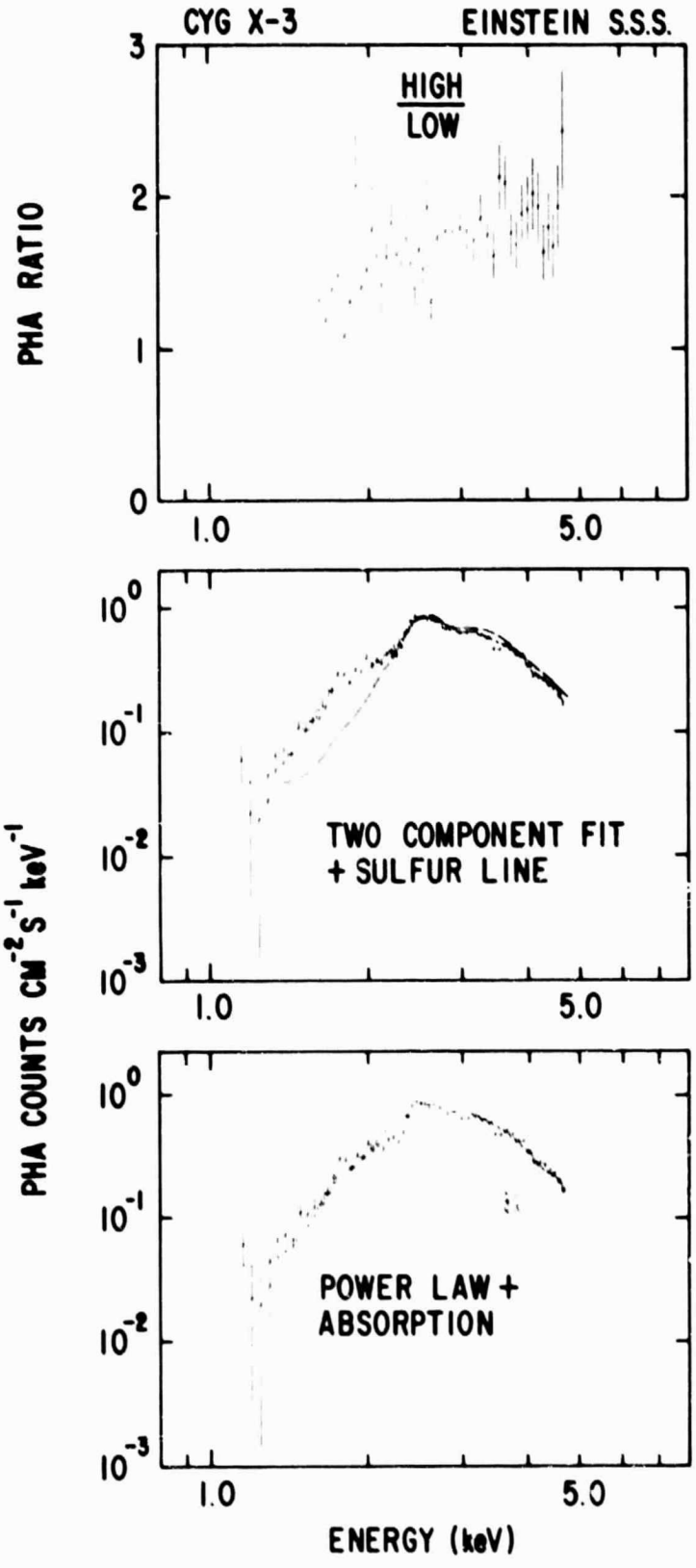
CYG X-3
EINSTEIN S.S.S.
HIGH
LOW
PHA RATIO
3
2
1
0
1.0
5.0
TWO COMPONENT FIT
+ SULFUR LINE
POWER LAW +
ABSORPTION
PHA COUNTS CM^{-2}S^{-1}keV^{-1}
10^{0}
10^{-1}
10^{-2}
10^{-3}
ENERGY (keV)

Figure 13

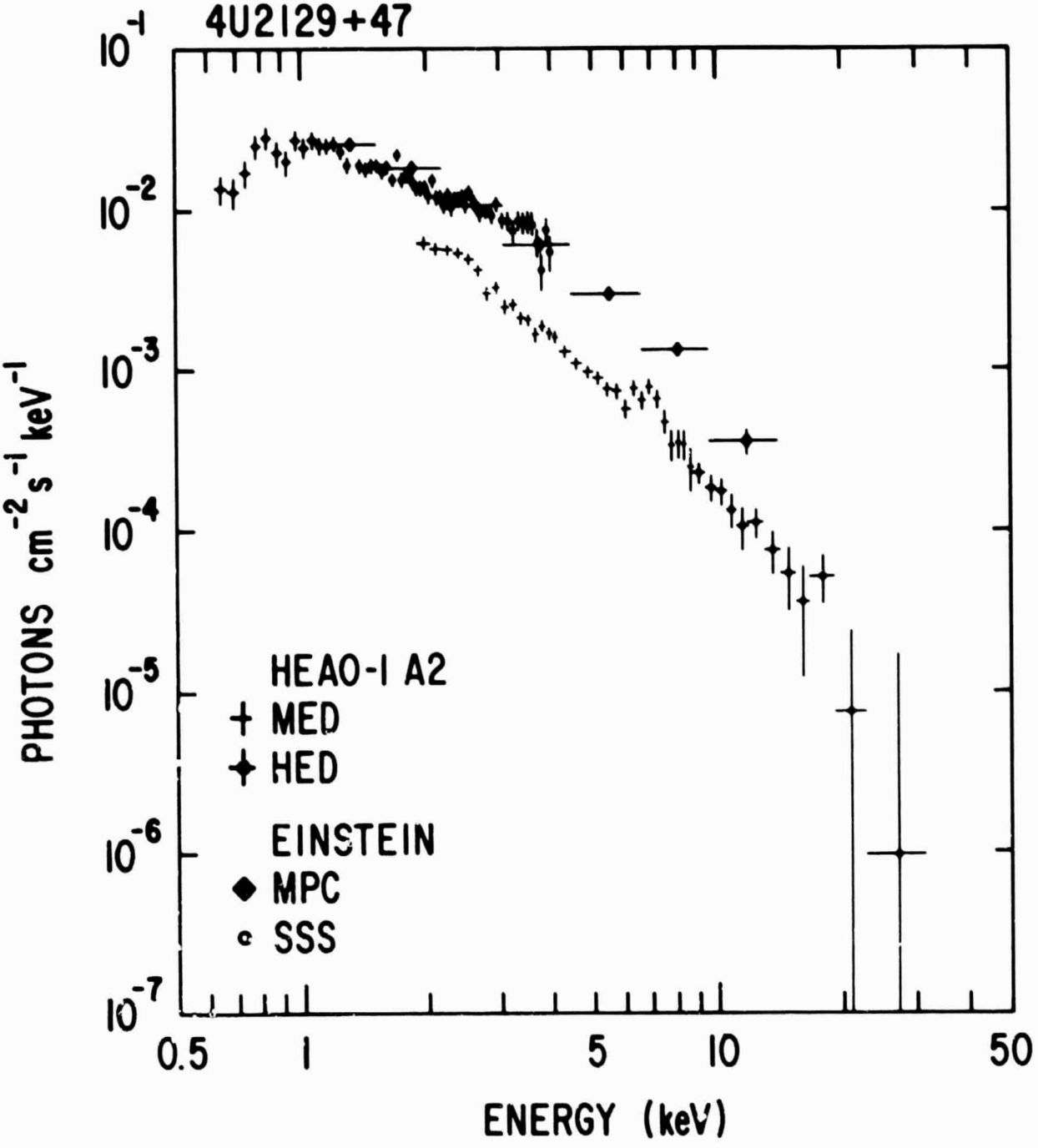
4U2129+47
HEAO-1 A2
MED
HED
EINSTEIN
MPC
SSS
PHOTONS cm^{-2} s^{-1} keV^{-1}
ENERGY (keV)
0.5
1
5
10
50

Figure 14

ADDRESS OF AUTHORS

S.S. HOLT and N.E. WHITE, Code 661, NASA/Goddard Space Flight Center, Greenbelt, MD 20771